Frequent occurrence of newly formed aerosol particles over wide geographical areas in the Arctic free troposphere and atmospheric boundary layer

David J. Simon[1], Jonas Schaefer[1], Jörg Hartmann[2], Benjamin Kirbus[3], Joshua Müller[3], Markus Hartmann[1], Bruno Wetzel[1], Laura Köhler[2], Anna-Marie Jörss[2], Kay Weinhold[1], Andreas Herber[2], Zsófia Jurányi[2], Silvia Henning[1], Gregory C. Roberts[4], Manfred Wendisch[3], Mira L. Pöhlker[1,3], and Frank Stratmann[1]

[1]Atmospheric Microphysics Department, Leibniz Institute for Tropospheric Research, Leipzig, Germany
[2]Alfred Wegener Institute, Helmholtz Centre for Polar and Marine Research, Bremerhaven, Germany
[3]Leipzig Institute for Meteorology, Leipzig University, Leipzig, Germany
[4]Scripps Institution of Oceanography, La Jolla, CA, USA

Correspondence: David J. Simon (simon@tropos.de)

Abstract. New particle formation (NPF) can impact the Arctic radiative energy budget since this region is particularly sensitive to changes in aerosol particle and cloud condensation nuclei concentrations. Prior measurements have predominantly investigated NPF in the Arctic atmospheric boundary layer (ABL), while vertically-resolved studies on newly formed aerosol particles remain scarce. Here, we present an analysis which suggests that NPF may take place throughout the entire lower Arctic troposphere. We have reached this conclusion by analyzing aerosol particle number size distribution data collected during a springtime aircraft campaign (BACSAM II) in the vicinity of Svalbard, the Fram Strait, and northern Greenland. We detected newly formed aerosol particles over distances of hundreds of kilometers, at various altitudes ranging from about 60 m to 3900 m, and identified four atmospheric scenarios for their occurrence: newly formed particles in the free troposphere, in the ABL over sea ice, in the vicinity of clouds, and in the ABL over ocean with sea ice floes. Our results indicate that regional Arctic atmospheric processes as well as long-range transport may play key roles in the formation of new particles. In particular, we deduce that one possible mechanism leading to free tropospheric NPF could be associated with warm-air intrusions.

1 Introduction

Aerosol particles are an important component of the global climate system (Forster et al., 2021). They enter the atmosphere either directly by primary emissions or are formed in situ by secondary aerosol particle formation from condensable gases (Seinfeld and Pandis, 2006). The latter process, which generates particles with diameters of initially a few nanometers, is termed new particle formation (NPF, Kulmala et al., 2004). Depending on the atmospheric thermodynamic conditions, subsequent growth can increase particle sizes to values large enough such that the particles may act as cloud condensation nuclei (CCN, Kulmala and Kerminen, 2008; Kerminen et al., 2018). CCN play a crucial role in cloud formation, affecting cloud life time, precipitation formation, and cloud albedo, thereby influencing Earth's radiative energy budget (Andreae and Rosenfeld, 2008;

Forster et al., 2021). Globally, about 50 % of CCN are estimated to result from NPF (Gordon et al., 2017; Pierce and Adams, 2009; Merikanto et al., 2009). In the Arctic, with commonly low background aerosol particle number concentrations, NPF is particularly important because of the high susceptibility of Arctic cloud formation (and hence cloud radiative forcing) to changes in aerosol particle and CCN number concentrations under low aerosol levels (Mauritsen et al., 2011; Leaitch et al., 2013; Carslaw et al., 2013; Gordon et al., 2017).

Currently, the Arctic is changing rapidly in response to global climate change (Box et al., 2019; Wendisch et al., 2017, 2023). Among others, these changes manifest in a substantial decrease of the Arctic sea ice cover, especially at the end of the Arctic summer in September (Stroeve et al., 2007). Furthermore, an increase of the near-surface air temperature is observed, which exceeds the global average warming by a factor of two to three (Wendisch et al., 2023). The processes causing the intensified response of the Arctic climate system to global climate change are commonly referred to as Arctic amplification (Serreze and Francis, 2006; Serreze and Barry, 2011; Wendisch et al., 2023). A changing Arctic also entails consequences for the Arctic aerosol population. For example, the decline of the sea ice cover affects both primary emissions from the ocean surface and secondary formation of aerosol particles (Willis et al., 2018; Schmale et al., 2021). Concerning the latter, enhanced emissions of precursor gases from open sea surfaces, leads, or through thinning sea ice have been reported and are expected to proceed as the sea ice fractures and retreats further (Cuevas et al., 2018; Galí et al., 2019). There is indirect evidence reported by Dall'Osto et al. (2017, 2018) who found a correlation between an increase of NPF events and decreasing sea ice extent. Furthermore, altered meridional transport may lead to enhanced aerosol particle and/or precursor transport into the Arctic, for instance, via warm-air intrusions (Dada et al., 2022; Wendisch et al., 2023, 2024), which are expected to occur more frequently in the future (Bintanja et al., 2020; Wendisch et al., 2025). Similarly, Heslin-Rees et al. (2020) showed that changed air circulation patterns resulted in an increased marine influence on the aerosol population at the Arctic Zeppelin station (Svalbard).

NPF has been observed in several locations Arctic-wide (Willis et al., 2018; Schmale and Baccarini, 2021). Most studies were based on measurements conducted during shipborne campaigns (e.g., Wiedensohler et al., 1996; Allan et al., 2015; Baccarini et al., 2020) or at ground-based stations including Alert, Villum, Zeppelin, Tiksi, and Utqiagvik (e.g., Leaitch et al., 2013; Croft et al., 2016; Asmi et al., 2016; Freud et al., 2017; Beck et al., 2021). These stations provide temporally extended datasets and enable the analysis of annual cycles and long-term trends. Yet, inherently, station- and ship-based measurements can hardly provide precise vertical information. However, data on the vertical distribution of NPF are crucial to identify and study key transport and formation processes, and ultimately, to assess the corresponding effects on the Arctic climate (Lee et al., 2019; Schmale et al., 2021; Price et al., 2023). There are remote sensing instruments such as lidar that can provide vertical information on aerosol particles, but these methods mostly miss the required sensitivity to reliably infer quantitative information on NPF. Consequently, to observe and analyze NPF, airborne measurements with balloons, helicopters, or aircraft appear indispensable (Garrett et al., 2002; Weber et al., 2003; Engvall et al., 2008; Khosrawi et al., 2010; Kupiszewski et al., 2013; Willis et al., 2016, 2017; Burkart et al., 2017; Pilz et al., 2024; Pohorsky et al., 2026). Despite these growing efforts to conduct vertically-resolved measurements on aerosol particles in general, and NPF in particular, data on the vertical distribution of NPF in the Arctic are still scarce (e.g., Burkart et al., 2017; Schmale et al., 2021; Pohorsky et al., 2026). Hence, the relative importance of the ABL and the free troposphere as sources of newly formed particles remains elusive. A number of studies reported on the

predominant occurrence of NPF close to the surface (Kupiszewski et al., 2013; Willis et al., 2016, 2017; Burkart et al., 2017; Willis et al., 2018), while other measurements detected NPF in the free troposphere as well (Weber et al., 2003; Khosrawi et al., 2010).

In this paper, rather than focusing on the process of NPF itself (i.e., the initial nucleation mechanism), we investigate the occurrence of newly formed particles produced by NPF, which have initial diameters of less than 20 nm (Kulmala et al., 2004). Here, we report on the frequent occurrence of these newly formed particles in the Arctic, found at various altitudes ranging from about 60 m to 3900 m above sea level. The corresponding data were collected during an aircraft campaign carried out in the Fram Strait, surrounding the Svalbard Archipelago, and in the vicinity of Villum Research Station (Station Nord) in Greenland in April 2024.

2 Methods

2.1 Aircraft campaign overview

The airborne campaign "Boundary layer and Aerosol and Cloud Study in the Arctic, based on aircraft and T-Bird Measurements II" (BACSAM II) was conducted from 5 April to 2 May 2024. We carried out eleven research flights (RFs) with the German research aircraft Polar 6 (P6, Wesche et al., 2016), operated by the Alfred Wegener Institute, Helmholtz Centre for Polar and Marine Research (AWI; see supporting information (SI) Fig. S1 for a map of all flight paths). With the operational base in Longyearbyen (Svalbard), target areas included the Fram Strait, the Svalbard Archipelago, and the vicinity of Villum Research Station in north-eastern Greenland. Flights were conducted between 7 and 29 April 2024. This time period was characterized by persistent warm air advection driven by low pressure systems south-west of Svalbard, resulting in above-average surface temperatures in Svalbard. Two exceptions with typical cold conditions and high pressure at the beginning of the campaign from 7 to 11 April and from 15 to 17 April occurred. Note that our sampling is potentially biased ~~towards~~ toward viable flight conditions, i.e., high visibility at Longyearbyen Airport. Furthermore, we mostly preferred cloud-free conditions in the target regions or elevated cloud layers (cloud base $\gtrapprox 200\,\mathrm{m}$), and no precipitation.

2.2 Aerosol measurements and detection of newly formed particles

Aboard the P6 aircraft, we measured aerosol particle number size distributions (PNSDs) with a mobility particle size spectrometer (MPSS, Wiedensohler et al., 2012, 2018). The custom-built MPSS measures the PNSDs in the particle diameter size range between 10 nm and 850 nm based on the electric mobility of aerosol particles with a time resolution of about 300 s. In this paper, we only use data up to 600 nm since on some measurement days arcing inside the differential mobility analyzer (DMA) led to artifacts in the PNSDs appearing at larger diameters. The system features a Vienna-type DMA (built by the ~~Leibniz Institute~~ Leibniz Institute for Tropospheric Research) and a condensation particle counter (CPC, TSI model 3760A, TSI Incorporated, USA). For further details on the MPSS system see Wiedensohler et al. (2012, 2018). The flow in the sampling tubing leading to the MPSS was manually adjusted depending on the true airspeed of the aircraft (typically $\approx 60\ \mathrm{m\,s^{-1}}$ during legs in the

target area and $\approx 90\ \mathrm{m\,s^{-1}}$ during transit flights) to achieve near-isokinetic sampling. As the onboard-temperature was significantly higher than the ambient temperature, the relative humidity of the sampled air in the aerosol inlet was below 40 %. Consequently, all reported particle diameters refer to dry conditions (Jurányi et al., 2025). All particle number concentration data have been corrected to standard conditions (1013 hPa and 273.15 K). Particle losses inside the sampling line from the aerosol inlet to the MPSS due to diffusion, sedimentation, turbulent inertial deposition, and inertial deposition in bends and contractions have been corrected for, based on calculations utilizing the particle loss calculator (Von der Weiden et al., 2009, Sect. S2).

Since the minimum diameter of aerosol particles that can be detected with our measurement instrumentation is 10 nm, it is not feasible to clearly identify the exact region where NPF occurred, i.e., where the process of the initial nucleation of particles with sizes of about 2 to 3 nm from condensable gases took place (Kulmala et al., 2004; Kerminen et al., 2018). Nevertheless, particle sizes of 10 nm still imply that these particles were newly formed by secondary particle formation (i.e., by NPF, Kulmala et al., 2004). We hence refer to these particles as newly formed particles and, in this paper, instead on the process of NPF, focus on the occurrence of such secondarily formed particles.

To detect newly formed particles, we fitted mono-modal, bi-modal, or tri-modal log-normal functions to the MPSS-measured

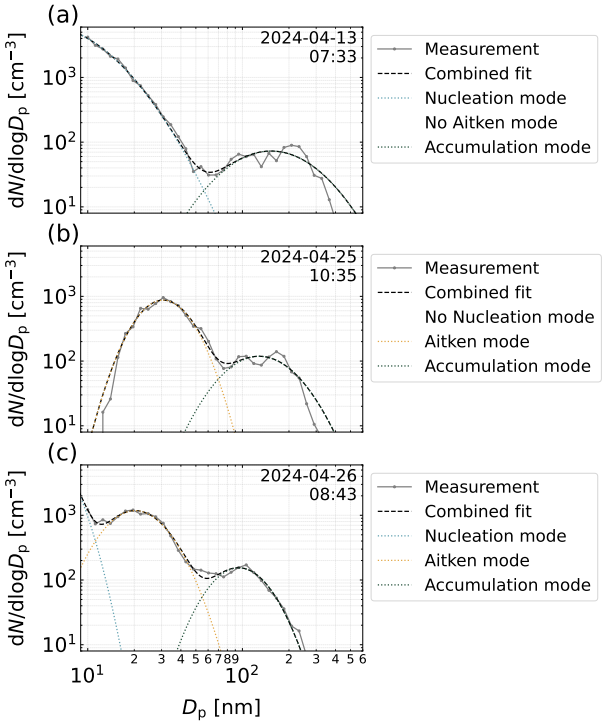


Figure 1. Examples of MPSS-measured PNSDs, showing nucleation and/or Aitken, and accumulation modes. The PNSDs in the panels **(a)** and **(c)** are considered as indicative for newly formed particles, while the measurement displayed in panel **(b)** shows no indication for newly formed particles.

PNSDs, with the different modes representing nucleation, Aitken, and accumulation modes, respectively. Following Kulmala et al. (2004), we refer to aerosol particles in the measured dry diameter range from below 10 nm to 20 nm as nucleation mode particles, from 20 nm to 90 nm as Aitken mode particles, and from 90 nm to 600 nm as accumulation mode particles. We consider an MPSS-measured PNSD as indicative for newly formed particles if the fitted distribution features a nucleation mode with a geometric mean diameter below 10 nm, i.e., a mode with a maximum below the lower size limit of the MPSS. The detection of newly formed particles was verified by visual inspection of the fitted PNSDs. Only distributions measured at a constant altitude were considered for quantitative analysis, i.e., PNSDs measured during the aircraft's ascents and descents were not taken into account in quantitative terms. Fig. 1 shows examples of three fitted PNSDs, with the data displayed in Fig. 1a and Fig. 1c indicating the presence of newly formed particles, and the data in Fig. 1b the absence of newly formed particles.

2.3 Meteorological measurements

A nose boom was installed at the tip of the aircraft to measure air pressure, temperature, and the three-dimensional wind vector. The nose boom features an Aventech five-hole probe to measure static, dynamic, and differential pressures to derive the wind vector from these data, and an open-wire Pt100 in an unheated Rosemount housing to record air temperature data. These data were measured with a time resolution of 100 Hz. Humidity data are available at 20 Hz from a Vaisala HMT333 in a Rosemount housing installed aboard the aircraft. Surface skin temperature data at 20 Hz are derived from measurements by a KT-19 infrared pyrometer (Heitronics KT-19.85 II). Position and altitude were measured by combining Global Positioning System (GPS) and Inertial Navigation System (INS) data, which were recorded at 100 Hz. See Hartmann et al. (2018) for further details on the instrumentation and data processing.

2.4 Backwards trajectory analysis

Backward trajectories were calculated from ERA5 wind fields (Hersbach et al., 2020) utilizing the Lagrangian analysis tool LAGRANTO (Sprenger and Wernli, 2015). The trajectories were initiated every minute along the flight track of the P6 at the corresponding flight altitude. The trajectories were calculated for 120 hours ~~backwards~~ backward in one minute time steps and several meteorological parameters from ERA5 were traced along the trajectory. Based on these parameters, we carry out an analysis of air mass history in Sect. 3. Among others, we determine the last contact of these air masses with clouds based on the specific cloud liquid water content ($CLWC$) and the specific cloud ice water content ($CIWC$). Here, we consider an air mass to have been in contact with a cloud if the total water content ($CWC = CLWC + CIWC$) exceeds the threshold of $CWC > 0.01\,\mathrm{g\,kg^{-1}}$ (McFarquhar and Cober, 2004; Moser et al., 2023, see Sect. S3).

3 Results and discussion

3.1 Geographical and vertical distribution of newly formed particles

Throughout the entire BACSAM II campaign, we frequently observed newly formed particles over large areas of the Arctic region studied (Fig. 2). Newly formed particles were detected during all eleven research flights, with the first observation of such particles on 7 April 2024, and the last on 29 April 2024. We encountered newly formed particles at various locations (approximately between 76°N to 85°N and 15°W to 26°E) and altitudes ranging from about 60 m to 3900 m above sea level (Fig. 2). The time periods during which we identified newly formed particles amount to an overall duration of about 10 hours and 30 minutes, which corresponds to approximately 29 % of the total measurement time (at constant altitude) of all research flights and a distance flown of about 2770 km.

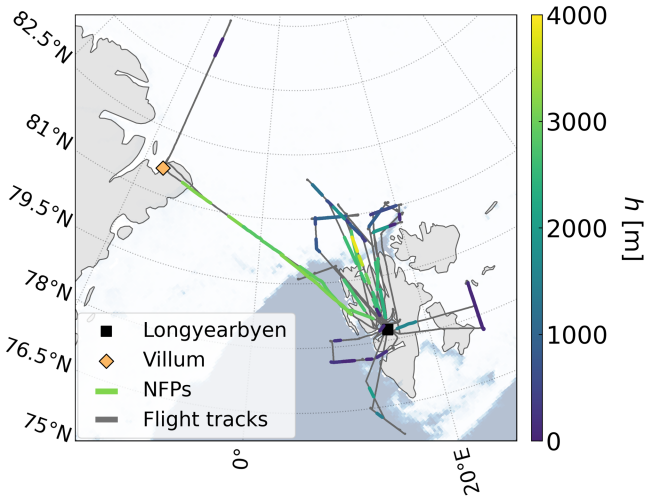


Figure 2. Geographical location and altitude at which newly formed particles (NFPs) were observed during the BACSAM II campaign. The flight tracks are shown in gray and the locations where newly formed particles were identified are color-coded by the corresponding flight altitude. The sea ice concentration is shown exemplary for 15 April 2024, during which we encountered newly formed particles at low altitudes over the ice-covered sea east of Svalbard (see Sect. 3.3). The corresponding sea ice data were retrieved from www.seaice.uni-bremen.de (Spreen et al., 2008).

Analyzing all measurements featuring newly formed particles in the course of our campaign, we could identify four distinct environmental conditions (based on the in situ data, see Sect. S3; Fig. 3). These cases include newly formed particles in the free troposphere (without clouds being present, Sect. 3.2), newly formed particles at low altitudes in the ABL over sea ice (Sect. 3.3), newly formed particles in the vicinity of clouds (Sect. 3.4), and newly formed particles inside the ABL over ocean with sea ice floes, i.e., the sea surface consisted of both open water and sea ice during the latter observations (Sect. S5). No indications ~~for~~ of the presence of newly formed particles were found within or near the ABL over open, completely ice-free ocean (Sect. S5).

Fig. 3a depicts the median size distributions of the PNSDs indicating the presence of newly formed particles, for each of the four environments. The highest particle number concentrations in the nucleation mode are found during observations of newly formed particles in the free troposphere. Inside the ABL over sea ice and in cloud vicinity, concentrations in the nucleation mode are smaller by a factor of roughly two. The smallest nucleation mode concentrations are observed inside the ABL over ocean with sea ice floes, with the concentrations being reduced by about one order of magnitude compared to the free tropospheric case.

In the accumulation mode, roughly similar concentrations are observed during newly formed particle-occurrence inside the ABL over ocean with sea ice floes and in cloud vicinity. Inside the ABL over sea ice, accumulation mode concentrations are slightly higher. The lowest accumulation mode concentrations are found in the free troposphere, with the mode being decreased by ~~a factor~~ factors of roughly two to four compared to the other cases.

The reader is referred to Sect. S4 and Fig. S3 regarding the related temperature and relative humidity conditions prevailing during observations of newly formed particles. We will discuss the observations for each of the four categories, which combined represent 92 % of all observations of newly formed particles, in more detail in Sect. 3.2, Sect. 3.3, Sect. 3.4, and Sect. S5.

~~About 45 % of all PNSDs featuring newly formed particles were detected in the free troposphere, corresponding to approximately 4 hours and 40 minutes of measurements (Fig. 3b, c) and distances flown of $\approx 1460\,\mathrm{km}$. About 16 % ($\approx$ 1 hour and 40 minutes, $\approx 350\,\mathrm{km}$) of all cases featuring newly formed particles were found in the ABL over sea ice, as well as 6 % ($\approx$ 40 minutes, $\approx 130\,\mathrm{km}$) in the ABL over ocean with sea ice floes. Approximately 25 % ($\approx$ 2 hours and 40 minutes, $\approx 630\,\mathrm{km}$) of all cases were observed in the vicinity of clouds (Fig. 3b, c). For approximately 8 % ($\approx$ 50 minutes, $\approx 200\,\mathrm{km}$) of all PNSDs featuring newly formed particles, the prevailing conditions could not unambiguously be identified, i.e., these cases could not clearly be assigned to one of the categories or to another separate category (Fig. 3b, c). They include flight sections during which clouds were present, but in contrast to the newly formed particles classified as in the vicinity of clouds, we did not carry out dedicated legs directly at cloud top or base, respectively. Also included are flight legs for which it could not unequivocally be determined if the legs were conducted inside or outside the ABL (see Sect. S3). **(a)** Median PNSD of all measurements showing newly formed particles (NFPs) associated with one of the environments described in the main text: newly formed particles in the free troposphere (Sect. 3.2), inside the ABL over sea ice (Sect. 3.3), in the vicinity of clouds (Sect. 3.4), and inside the ABL over ocean with ice floes (Sect. S5). **(b)** Total measurement times per altitude (grouped into height bins with a width of 100 m) showing the absence of newly formed particles as well as times during which newly formed particles were detected for the different environments. **(c)** For convenience, this subplots shows the duration of newly formed particle-occurrence (NFP-occurrence) per measurement altitude again for the different categories, i.e., the same NFP data as in the first panel. The NFP data here and in panel (b) are shown as stacked bars. Note the different range of the x-axis compared to (b). **(d)** Relative frequency of NFP-occurrence per measurement altitude (irrespective of category), i.e., NFP-occurrence divided by total measurement time. The hatched bars at altitudes higher than 3500 m indicate that here only one full PNSD measurement was conducted within each altitude bin, while below 3200 m on average 14 MPSS scans were carried out at each altitude, with a maximum of 79 scans between 60 and 100 m (Fig. 3a).~~ As mentioned earlier, newly formed particles were detected in a wide range of altitudes between approximately 60 m and 3900 m (Fig. 3~~b–d~~b). Here, 60 m and 3900 m correspond to the minimum

and maximum flight altitudes at which measurements were carried out (Fig. 3b). Consequently, we cannot rule out that newly formed particles could be present at altitudes even higher than 3900 m in the target regions during our campaign.

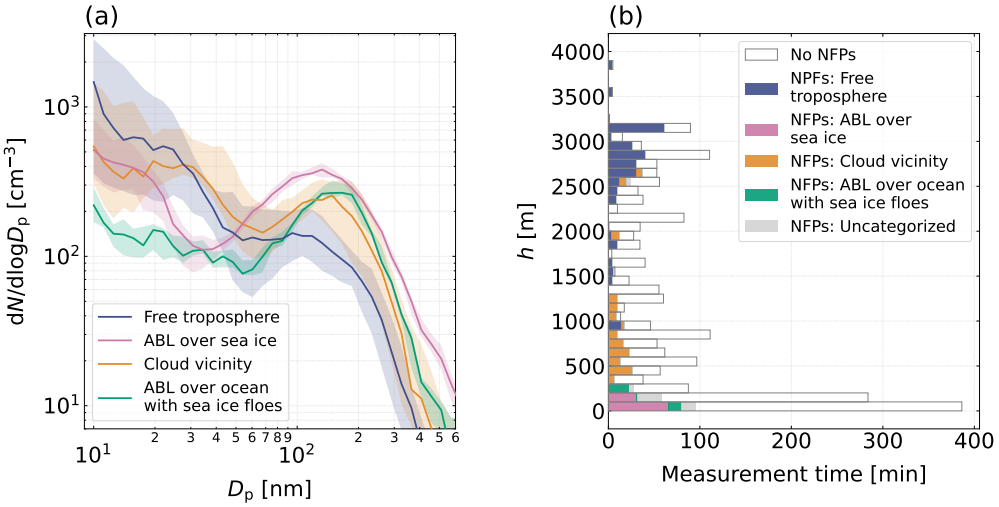


Figure 3. **(a)** Median PNSD of all measurements showing newly formed particles (NFPs) associated with one of the environments described in the main text: newly formed particles in the free troposphere (Sect. 3.2), inside the ABL over sea ice (Sect. 3.3), in the vicinity of clouds (Sect. 3.4), and inside the ABL over ocean with ice floes (Sect. S5). **(b)** Total measurement time per altitude (grouped into altitude bins with a width of 100 m). Colored bars illustrate the duration of newly formed particle-occurrence in each altitude bin, labeled by the different environments. White bars indicate the absence of newly formed particles. The data are shown as stacked bars.

In the free troposphere, newly formed particles were detected at altitudes between about 900 m and 3900 m (Fig. 3~~d presents an overview of the frequency of occurrence of~~ b). These observations amount to measurement times of approximately 4 hours and 40 minutes, corresponding to distances flown of $\approx 1460\,\mathrm{km}$. Inside the ABL over sea ice, at altitudes between roughly 60 m and 200 m, newly formed particles were identified during about 1 hour and 40 minutes of measurements ($\approx 350\,\mathrm{km}$), and inside the ABL over ocean with sea ice floes, at altitudes between 60 m and 300 m, during approximately 40 minutes ($\approx 130\,\mathrm{km}$). During about 2 hours and 40 minutes ($\approx 630\,\mathrm{km}$) of measurements in the vicinity of clouds, newly formed particles ~~during our campaign~~were observed. Here, ~~we show the relative frequency of occurrence per altitude bin, defined as the duration~~ these particles were found at altitudes between 300 m and 2700 m (Fig. 3b).

Table 1 summarizes the durations of newly formed particle-occurrence for the four environments. Furthermore, based on ERA5 reanalysis data, we present total measurement times spent in the free troposphere, in the ABL over sea ice and over ocean with sea ice floes, and in cloud vicinity throughout the campaign (see Sect. S3 for details). Additionally, relative frequencies of occurrence of newly formed ~~particle-observations per altitude, normalized by the total time of all PNSD measurements within this altitude bin. The frequency values show a rather variable vertical distribution. For example, in the lowest 300 m, roughly 25 % of all measured PNSDs featured~~ particles for each environment are provided in Table 1. As discussed in Sect. S3, the ERA5-based values are associated with large uncertainties. Consequently, the total measurement times throughout the

Table 1. Overview of total measurement time as well as duration and frequency of newly formed particle-occurrence (NFP-occurrence) for the four environments.

	Free troposphere	ABL irrespective of surface	ABL over sea ice	ABL over ocean with sea ice floes	Cloud vicinity
Duration of NFP-occurrence (based on in situ data)	4 h 40 min	2 h 20 min	1 h 40 min	40 min	2 h 40 min
Total measurement time [1] (based on ERA5)	25 h 10 min	8 h 10 min	3 h 30 min	1 h	2 h 10 min
Frequency of NFP-occurrence [1]	19 %	29 %	48 %	67 %	($>$ 100 %) [2]

1: Note that the ERA5-based values (i.e., total measurement time and, consequently, frequency of NFP-occurrence) should be considered semi-quantitatively only (see the discussion in the main text and Sect. S3 for details).

2: Nonphysical value, resulting from ERA5 not always predicting clouds throughout all legs which are known to have been carried out in cloud vicinity, according to the in situ observations. Considering those times based on the in situ data instead of the ERA5-based values, a frequency of about 73 % can be reported.

campaign as well as the frequencies of occurrence should be interpreted solely semi-quantitatively and only provide a very rough estimate.

It should be noted that, for all case studies described below, as well as for the assignment of measurement periods featuring newly formed particles ~~. At altitudes between about 2500 m and 3200 m, up to almost 75 % of PNSDs indicate the presence of~~ to the four categories free troposphere, cloud vicinity, ABL over sea ice, and ABL over ocean with sea ice floes, we only considered flight sections for which the prevailing conditions could be clearly identified based on the in situ data. If newly formed particles were detected but either, e.g., the ABL height could not be determined for the target region or the absence/presence of clouds close to the aircraft could not be verified, these observations are assigned to the unclassified cases (Sect. S3). Such observations represent 8 % of all PNSDs featuring newly formed particles (~~Fig. 3d). Note that~~ $\approx$ 50 minutes, $\approx$ 200 km of measurements).

Naturally, during the campaign, sampling times and consequently ~~number~~ numbers of PNSDs measured, as well as distances flown at certain altitudes, were not evenly distributed over the investigated altitudes, geographical locations, and synoptic conditions (Fig. 3b). For example, while measurements in the lowest 100 m were carried out for a total duration of almost 400 min (over a distance of about 1480 km), measurements at 3500-3600 m and 3800-3900 m were ~~solely~~ merely performed during one research flight, and at each altitude range for merely 5 to 10 min (27 to 54 km, to feature one full MPSS scan; ~~hatched bars in~~ Fig. 3~~d~~b). The values of duration and relative frequency of newly formed particle-occurrence reported in this section are thus not intended to constitute representative values for the lower Arctic troposphere. They rather provide a rough overview and represent (semi-quantitative) statistics of the observations made during the BACSAM II campaign. ~~Despite these limitations , we additionally present statistics concerning the total measurement times spent in the free troposphere, in the ABL over sea ice and over ocean with sea ice floes, and in cloud vicinity throughout the campaign in Sect. S3, based on ERA5 reanalysis~~

data. Further, relative frequencies of occurrence of newly formed particles for these environments are provided. The values are associated with rather large uncertainties and can therefore only provide a very rough estimate (see Sect. S3 for details). Nevertheless, Nevertheless, despite these limitations with respect to the statistical analysis, our measurements clearly demonstrate that newly formed particles were frequently found throughout the lower Arctic troposphere, and suggest that NPF in the Arctic occurred across large geographical areas and over a wide range of altitudes during our campaign in April 2024.

To further elucidate the atmospheric scenarios under which newly formed particles were observed, and to gain insights into potential precursor gases and their origins, in the following sections, the results of case studies focusing on newly formed particles in the free troposphere, inside the ABL over sea ice, and in the vicinity of clouds will be presented. First, specific examples for these scenarios will be given. Second, to put the given examples into a larger perspective, we will discuss respective backward trajectory analyses for all air masses featuring newly formed particles for each of these three environments. Regarding the presence of newly formed particles inside the ABL over ocean with sea ice floes, as well as the absence of such particles inside the ABL over completely ice-free ocean, the backward trajectory analysis required is somewhat different compared to the other three cases (for example, due to the prevailing meteorological conditions, e.g., air masses passing over the island of Spitsbergen, see Sect. S5 for details). To keep the main text both consistent and concise, these latter observations (inside the ABL over ocean with sea ice floes and over open ocean) are discussed comprehensively in the SI in Sect. S5.

3.2 Newly formed particles in the free troposphere

Here, as an illustrative example, we present results concerning newly formed particles in the free troposphere which were encountered on 13 April 2024 during RF04 while transiting from Longyearbyen (Svalbard) to Villum Research Station (northern Greenland) at an altitude of 2890 m (Fig. 4a).

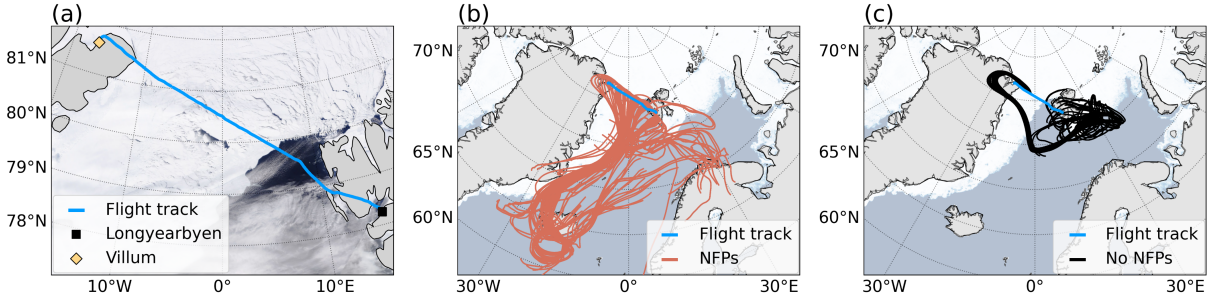


Figure 4. (a) Flight track of RF04 on 13 April 2024. The Moderate-resolution Imaging Spectroradiometer (MODIS)-TERRA satellite image was retrieved from https://wvs.earthdata.nasa.gov. **(b)** Five-day backward trajectories associated with newly formed particles (NFPs) along the section of the flight trackshown in Fig. 5. **(c)** Five-day backward trajectories connected to PNSD measurements featuring no newly formed particles. The sea ice concentration data shown in the subplots (b) and (c) were retrieved from www.seaice.uni-bremen.de (Spreen et al., 2008).

In the two days ahead of the flight, a low pressure system located over the east coast of Greenland advected warm and moist air

over the sea ice edge in the Fram Strait (Fig. 4b). Within this warm-air intrusion, North Atlantic ABL air was lifted up to the free troposphere. The uplifting over the sea ice edge was accompanied with the formation of precipitating clouds, which dissipated before sampling of the air mass. Consequently, the sampled free tropospheric air was cloud-free. The cumulus clouds visible in the satellite image in Fig. 4a capped the marine ABL, which was located more than 2 km beneath the flight track. Therefore, we expect no influence of these low-level clouds on our measurements in the free troposphere. In addition to the southerly air masses from the Atlantic, air masses originating at higher latitudes close to Svalbard were probed during RF04 (Fig. 4c).

During the time period from about 6:23 to 7:40 UTC, flying at high altitudes ($\approx$ 2890 m), and covering a distance of about 409 km, we encountered elevated number concentrations in the lower MPSS size bins (Fig. 5). The measured PNSDs featured a sharp decline in the size range from 10 nm to about 60 nm, i.e., we observed the "upper" end of a pronounced nucleation mode (see Fig. S8 for the related median PNSD). Detected particle number concentrations in the size range from 10 nm to 20 nm reached on average values of about $N_{10-20} \approx 778\ \mathrm{cm}^{-3}$, which constituted about 68 % of the total particle number ~~concentration~~ concentrations measured in the range from 10 nm to 600 nm (Fig. 5c). In other words, we detected newly formed particles in the Arctic free troposphere across a large geographical area.

For the time period 7:40 to 8:19 UTC, encountered PNSDs featured no distinct nucleation mode, and number concentrations in the size range from 10 nm to 20 nm were substantially lower ($N_{10-20} \approx 27\ \mathrm{cm}^{-3}$, 17 % of the total MPSS-measured number ~~concentration~~concentrations, Fig. 5c), i.e., no newly formed particles were present. Notably, the newly formed particles observed during the first part of the transit flight were associated with air masses originating from lower latitudes which were transported into the Arctic within a warm-air intrusion (Fig. 4b), while in the northerly air masses no newly formed particles

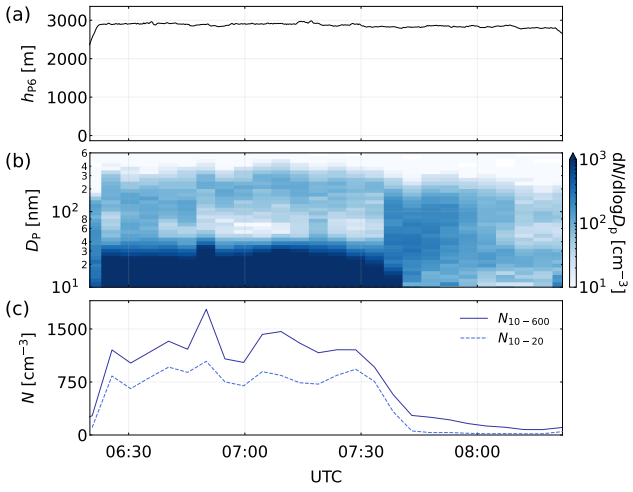


Figure 5. **(a)** P6 altitude during RF04 on 13 April 2024. **(b)** MPSS-measured PNSD. **(c)** Integral particle number concentrations in the total measured size range (10 nm $\leq D_\mathrm{p} \leq$ 600 nm, solid line) and in the nucleation mode size range (10 nm $\leq D_\mathrm{p} \leq$ 20 nm, dashed line), respectively.

were detected (Fig. 4c).

Backward trajectory analysis of all air masses featuring newly formed particles in the free troposphere

To further elucidate free tropospheric newly formed particles, which we observed on eight different days, considering all research flights performed during BACSAM II, and utilizing backward trajectories, a systematic analysis of free tropospheric air mass history was carried out. We investigated both free tropospheric air masses that show clear signs of newly formed particles, and free tropospheric air masses that exhibit no indications of newly formed particles. Every minute of each flight, we initiated a five-day backward trajectory at the pressure altitude of the aircraft. Hence, the air sampled during one PNSD measurement, which lasts for approximately 5 minutes and indicates either the presence or absence of newly formed particles, is represented by five backward trajectories. The results of the analysis are presented in Fig. 6, which depicts median values of meteorological and geographical parameters along the trajectories of all flight sections carried out in the free troposphere throughout the campaign.

Predominantly, air masses featuring newly formed particles in the free troposphere originated further south compared to air masses with no indications ~~for~~ of free tropospheric newly formed particles, and gradually moved poleward at high altitudes during the five days prior to arrival (Fig. 6a-c). Initially, these air masses connected to newly formed particle were warmer and contained more moisture (Fig. 6d, f). Higher values of northward integrated water vapor transport (IVT_{north}) show that in the whole column more water vapor was transported poleward for cases when newly formed particles were observed in the Arctic free troposphere (Fig. 6g). About 60 hours before arrival, temperatures of air masses linked to newly formed particles started to decrease, and between 24 to 48 hours prior to arrival, specific humidities decreased as well, while for the trajectories featuring no newly formed particles, the specific humidities remained rather constant throughout the last five days. Consequently, air masses associated with newly formed particles became colder and less humid compared to air masses showing no signs of free tropospheric newly formed particles. The latter, i.e., the decrease of specific humidity, might be caused by the formation of precipitating clouds, as already mentioned in the case study above. Considering the 75th percentile of the specific humidity in addition to the median values, the analysis suggests that some precipitation already set in up to roughly 100 hours prior to arrival for trajectories connected to newly formed particles. About 80 % of all backward trajectories linked to free tropospheric newly formed particles were in contact with clouds on their way to the measurement location during the previous five days, as well as about 70 % of the backward trajectories featuring no newly formed particles (Fig. 6i). However, no clouds were present during the last 24 hours before the measurement for the air masses featuring newly formed particles. For approximately 50 % of the respective trajectories the last contact with clouds occurred between about 24 to 48 hours prior to arrival (Fig. 6i). The decrease in specific humidity during the same time period (Fig. 6f) already mentioned above indicates that the removal of clouds, at latest 24 hours prior to arrival, could (partly) be caused by precipitation. None of the backward trajectories featuring newly formed particles resided in the ABL ~~for the last 12~~ during the last 48 hours prior to arrival~~at the track of the P6, and less than 2 % of these trajectories passed through the ABL in the last 54 hours. About~~ , and about 70 % of the backward trajectories had no contact with the ABL for the last five days (Fig. 6h).

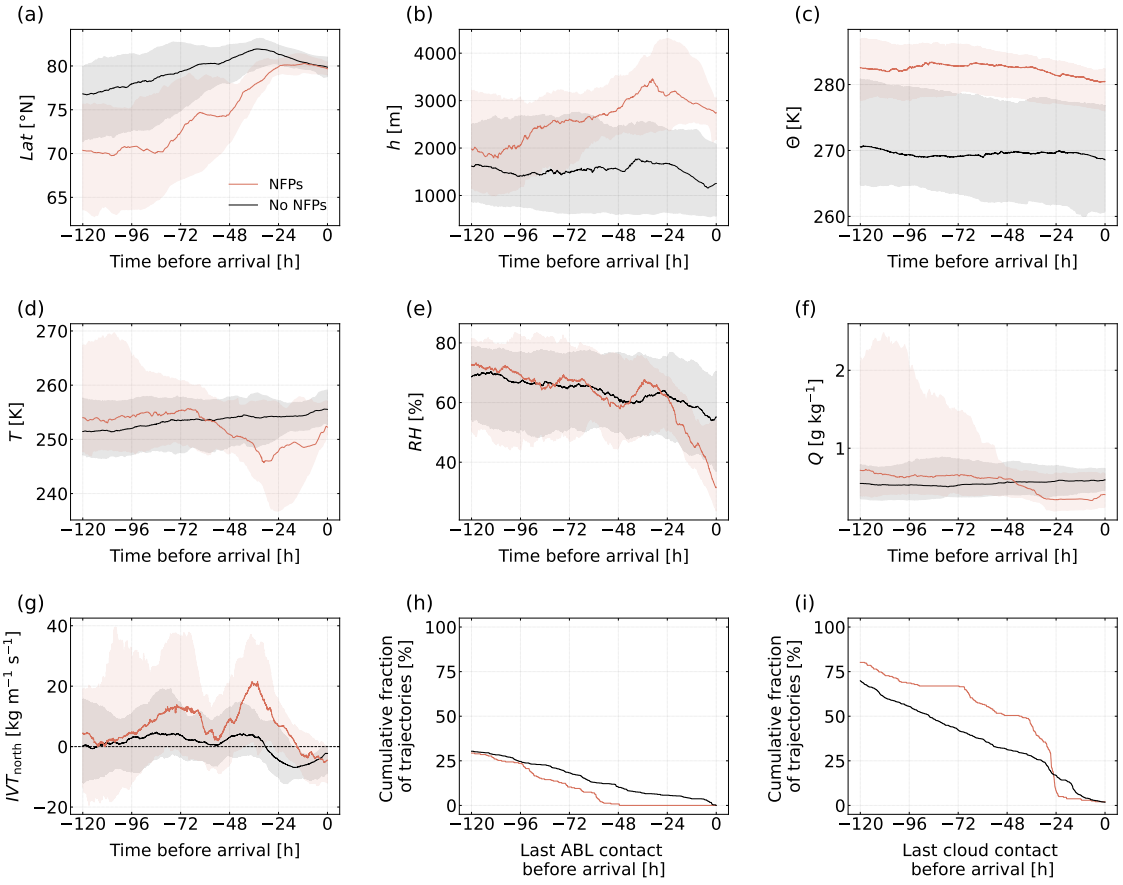


Figure 6. Comparison of geographical and meteorological parameters along the backward trajectories of flight sections in the free troposphere between trajectories connected to the presence (red) and absence (black) of newly formed particles (NFPs). Shown, as a function of time prior to arrival at the measurement location, are median values (solid lines) and interquartile ranges (shaded areas) of **(a)** latitude Lat, **(b)** altitude h, **(c)** potential temperature Θ, **(d)** absolute temperature T, **(e)** relative humidity RH, **(f)** specific humidity Q, and **(g)** northward integrated water vapor transport IVT_{north}. The last two subplots show the cumulative fraction of the last contact of the trajectories with the **(h)** ABL and **(i)** clouds. Note that if the cumulative fraction does not increase to 100 % at $t = -120\,\mathrm{h}$, this indicates that a fraction of the trajectories was not in contact with the ABL/clouds during the last five days (the maximum time span the calculated trajectories cover).

These findings suggest that the cases of newly formed particles in the Arctic free troposphere observed during our campaign are predominantly connected to poleward transport of warm and moist air, as occurring, e.g., during warm-air intrusions (Wendisch et al., 2024). Furthermore, because the trajectories overwhelmingly remained in the free troposphere during the transport to the measurement region, the results indicate that the precursor gases involved in the formation of these particles originated from long-range transport from lower latitudes, with NPF very likely occurring in the Arctic free troposphere. Such a transport pathway for precursor gases resulting in free tropospheric NPF has already been suggested in a modeling study by Price et al. (2023).

The above findings imply a potential role for clouds in the transport and possibly transformation of precursors, e.g., through releasing precursor gases from evaporating cloud droplets (Weber et al., 2001; Wehner et al., 2015). Precipitation caused by these clouds might have also increased the probability for NPF to occur by removing large aerosol particles, thus decreasing the pre-existing particle surface area and consequently reducing scavenging of gaseous precursors and newly formed particles (Perry and Hobbs, 1994; Weber et al., 2001). Interestingly, already Khadir et al. (2023) observed a consistently positive correlation between nucleation mode particles and precipitation rate within the air mass during the transport to Zeppelin research station from about 24 to 96 hours prior to arrival, and mostly negative correlations between precipitation rate and nucleation mode particles in the last 12 hours. These results were found for data recorded from March to May, i.e., for a similar season as for our campaign, and covered the years from 2010 to 2019. Although with our dataset we cannot robustly identify significant correlations similar to Khadir et al. (2023), our analysis likewise suggests that precipitating clouds (occurring until about 24 hours prior to the measurement) might create favorable conditions for NPF to occur by releasing precursors and reducing the existing particle surface area (i.e., decreasing the condensation sink).

The presence of newly formed particles in the Arctic free troposphere has occasionally been reported before (Weber et al., 2003; Khosrawi et al., 2010). For example, Weber et al. (2003) conducted systematic aircraft measurements in the free troposphere of the Canadian Arctic from January to May 2000. During one of 38 research flights, they observed one clear NPF event at an altitude of approximately 4200 m over the Canadian Arctic Archipelago. During the other 37 flights of their campaign, no indications ~~for~~ of NPF occurring at high altitudes were found. Similarly, Khosrawi et al. (2010) detected one NPF event in the upper free troposphere at an altitude of 7000 m over Storfjoden (Svalbard). Below 4000 m, nucleation mode particles were reported to occur quite frequently during their campaign centered around Svalbard in May and June 2004. Yet, no further altitude-resolved information or discussion discriminating between ABL and free tropospheric NPF was provided, except for one case study, where in addition to the NPF event at 7000 m, nucleation mode particles were found inside the ABL. Analyzing measurements conducted with a tethered balloon system, Pilz et al. (2024) reported enhanced number concentrations of aerosol particles in the size range from 12 nm to 150 nm concurrently with low concentrations of particles larger than 150 nm in the summertime Central Arctic during the Multidisciplinary drifting Observatory for the Study of Arctic Climate (MOSAiC) expedition. The authors hypothesized that NPF taking place aloft lead to these elevated concentrations of smaller particles but were unable to constrain potential sources and associated processes due to a limited maximum measurement altitude of 1000 m and because of missing PNSD measurements. Utilizing helicopter (Kupiszewski et al., 2013) and aircraft measurements (Burkart et al., 2017; Willis et al., 2016, 2017), a number of studies reported generally lower concentrations of nucleation mode particles in the Arctic free troposphere compared to the ABL. In these studies, however, several NPF events were observed near the surface.

Similar to the previous observational results, our data show that newly formed particles occurred in the free troposphere. Notably, our observations suggest that these particles prevailed over distances of several hundreds of kilometers.

Whether the formation of clouds and thus cloud radiative forcing could be affected by the presence of newly formed particles in the free troposphere following their potential growth to CCN sizes, remains to be assessed and is both beyond the scope of this article and not feasible with the present dataset. In this regard, e.g. Leck and Bigg (1999); Bigg and Leck (2001) described

that during their summertime campaign over the central Arctic Ocean, highly stable conditions prevented mixing between the free troposphere and the ABL. Pointing toward the importance of free tropospheric particles for cloud formation, however, Pohorsky et al. (2026) reported that free tropospheric sources of CCN were required to explain measured cloud droplet number concentrations. This is in line with a large-eddy simulation study by Igel et al. (2017) which demonstrated that elevated aerosol particle layers in the free troposphere could be entrained into the cloud-topped ABL by cloud-induced mixing.

Overall, our results lead us to the hypothesis that meridional transport in combination with cloud processing and precipitation, as occurring in connection with, e.g., warm-air intrusions, may play an important role in free tropospheric Arctic NPF by delivering the ingredients (precursor gases including water vapor) to locations (high altitudes) with favorable conditions (intense solar radiation, low temperatures, small pre-existing particle surface area) for NPF.

3.3 Newly formed particles inside the atmospheric boundary layer over sea ice

Inside the ABL, newly formed particles were detected, e.g., on 15 April 2024 during RF05 while flying east of Svalbard at low altitudes (approximately 70 m and 155 m) over sea ice, where cracks as well as open and partly refrozen leads were present (Fig. S9). The associated flight track is shown in Fig. 7a, with Fig. 7b, c depicting the backward trajectories for the air masses encountered along the flight track.

The area investigated was subject to the anti-cyclonic flow around a high pressure system north of Svalbard, causing cold air advection from the central Arctic to the target region. This meteorological situation resulted in air masses that exclusively originated in the high Arctic and traveled toward the P6 flight track from higher latitudes over sea ice-covered regions (Fig. 7b, c). All the way between waypoint 1 (WP1) and WP3, over a distance of about 115 km, clear sky conditions prevailed (Fig. 7a). The presence of newly formed particles is indicated by the occurrence of a distinct nucleation mode, i.e., elevated aerosol particle number concentrations in the lower size bins of the PNSDs, which we observed during three consecutive legs at altitudes of

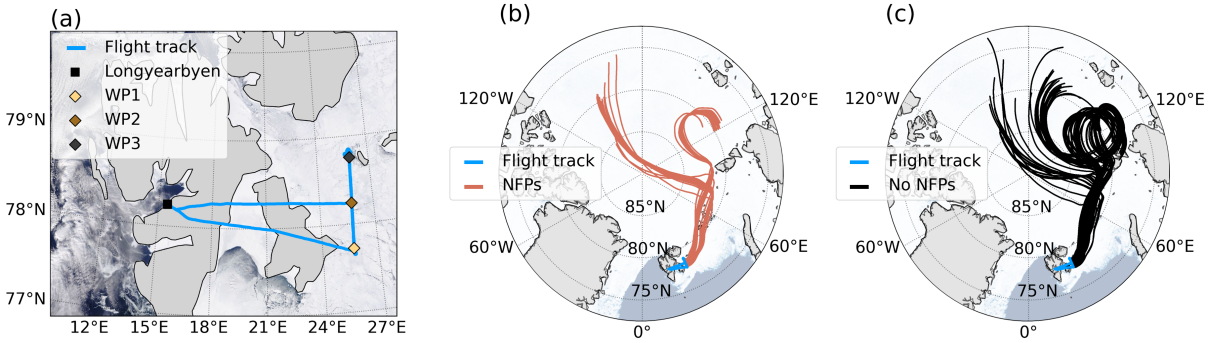


Figure 7. (a) Flight track of RF05 on 15 April 2024. The MODIS-TERRA satellite image was retrieved from https://wvs.earthdata.nasa.gov. **(b)** Five-day backward trajectories associated with newly formed particles (NFPs) along the section of the flight track shown in Fig. 8. **(c)** Five-day backward trajectories connected to PNSD measurements featuring no newly formed particles. The sea ice concentration data shown in the subplots (b) and (c) were retrieved from www.seaice.uni-bremen.de (Spreen et al., 2008).

$\approx 70\,\mathrm{m}$ and $\approx 155\,\mathrm{m}$ between WP1 and WP3 (Fig. 8). Mean number concentrations in the nucleation mode size range reached $N_{10-20} \approx 206\ \mathrm{cm}^{-3}$ (time period 10:03 to 10:39 UTC), $N_{10-20} \approx 185\ \mathrm{cm}^{-3}$ (11:08 to 11:22 UTC), and $N_{10-20} \approx 125\ \mathrm{cm}^{-3}$ (12:17 to 12:40 UTC), accounting for about 40 %, 38 %, and 31 % of the total MPSS-measured aerosol particle number concentrations. In contrast, during the leg at $\approx 850\,\mathrm{m}$ altitude (11:30 to 12:00 UTC) between WP1 and WP3, as well as during the transit to and from the target region at $\approx 1360\,\mathrm{m}$ altitude, the PNSDs featured no nucleation mode and, accordingly, low number concentrations in the sub-20 nm size range (Fig. 8, $N_{10-20} \approx 3\ \mathrm{cm}^{-3}$, 1 % of the total MPSS-measured particle number concentration at 850 m).

From the vertical profiles of potential temperature obtained during the ascents and descents at WP1, WP2, and WP3 (Fig. 8a), we determine an ABL height of about 190 m in the region of interest (see Fig. S10). Thus, the three legs at 70 m and 155 m, during which newly formed particles were detected, were carried out inside the ABL, while the leg at higher altitude ($\approx 850\,\mathrm{m}$), as well as the transits to and from the region of interest, took place in the free troposphere.

Integral aerosol particle number concentrations in the total measured size range (10 nm to 600 nm) and in the size range from 10 nm to 20 nm decreased from WP1 to WP3, i.e., from south to north (Fig. 7a, Fig. 8). The spatial variability of the number concentration of nucleation mode particles points toward newly formed particles as the result of regional formation rather than long-range transport. Nucleation mode particles have short atmospheric residence times due to their high diffusion, coagulation with larger particles, and condensational growth out of the nucleation mode size (e.g., Pruppacher and Klett, 2010; Wallace and

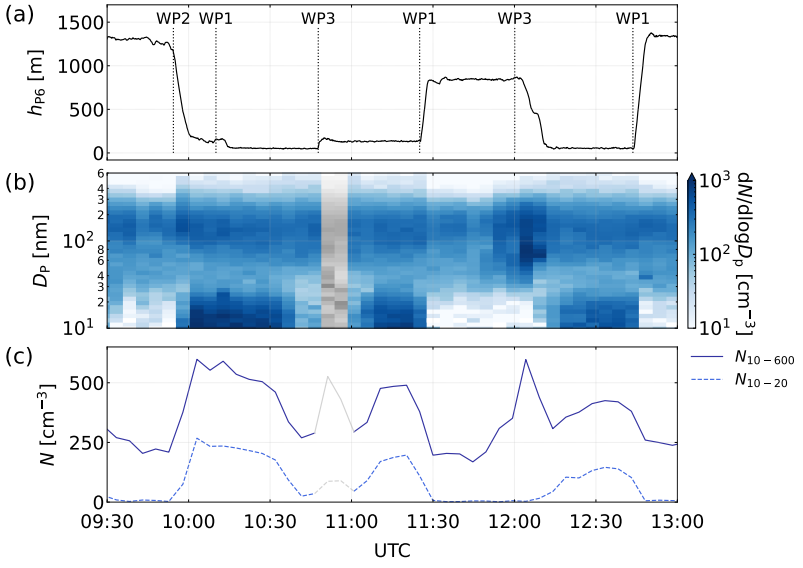


Figure 8. **(a)** P6 altitude during RF05 on 15 April 2024. **(b)** MPSS-measured PNSD. **(c)** Integral particle number concentrations in the total measured size range ($10\ \mathrm{nm} \leq D_\mathrm{p} \leq 600\ \mathrm{nm}$, solid line) and in the nucleation mode size range ($10\ \mathrm{nm} \leq D_\mathrm{p} \leq 20\ \mathrm{nm}$, dashed line), respectively. The data measured from 10:51 to 11:01 UTC are grayed out in panels (b) and (c) since erroneous measurements due to possible sampling of aircraft exhaust cannot be ruled out.

Hobbs, 2006). These effects tend to smooth out concentration gradients of such small particles, thereby making a contribution from long-range transport to the observed events less likely (Kupiszewski et al., 2013).

Interestingly, the particle number concentrations in the nucleation mode size range from 10 nm to 20 nm recorded during the legs inside the ABL between WP1 and WP3 (i.e., in the same area) decreased not only spatially, but also over time (Fig. 8c). In addition to the integral values shown above, Fig. S11 depicts median PNSDs for each of the three legs close to the surface individually, which likewise shows that number concentrations of particles in the nucleation mode reduce over time. This temporal variability points toward a regional source as well, since it suggests that we observed an NPF event that becomes weaker throughout the day. However, we are not able to unambiguously resolve if the precursors involved in NPF originated directly from the sea ice-covered measurement region, with various cracks and leads being present (Fig. S9), or if the precursors were transported to the target area from the higher Arctic. But, in our view, it appears feasible to conclude that the spatial and temporal variability of the newly formed particles encountered here (i.e., the decrease of sub-20 nm particles from WP1 to WP3 and throughout the day) and the similar origin of air masses featuring newly formed particles (Fig. 7b) and air masses without newly formed particles (Fig. 7c) rather indicate a regional source.

Backward trajectory analysis of all air masses featuring newly formed particles in the atmospheric boundary layer over sea ice

To further investigate the occurrence of newly formed particles inside the ABL over sea ice, an analysis of air mass history was carried out for the respective observations made during our campaign. Newly formed particles inside the ABL over sea ice were found twice, i.e., on 15 April (case study) and on 13 April for approximately 15 min north of Villum Research Station (see Fig. 2). Fig. 9 presents the results of the backward trajectory analysis carried out for both events.

Both days were characterized by cold air masses from northern latitudes which traveled over sea ice-covered regions (median sea ice concentration values between ≈ 95 % and 100 %, Fig. 9a, b, e). The air masses featured low specific humidities, but, due to cold temperatures, high relative humidities (w.r.t. water, Fig. 9e-g). Furthermore, the data suggest that all trajectories resided inside the ABL during the last 24 hours (Fig. 9i) before arriving at the P6, providing the possibility for precursor uptake. For about 60 % of the trajectories, the last cloud contact occurred approximately 24 h before arrival in the target region (Fig. 9j). Roughly 15 % of the trajectories were not influenced by clouds on their way to the measurement location during the last five days, including 80 % of all trajectories on 13 April. For both days, the trajectories descended during the last five days, with the lowest altitude along the trajectories reached just before arrival at the aircraft (Fig. 9c). The descent of the backward trajectories again indicates rather regional precursor sources as the gases are very likely emitted from the surface.

NPF in the Arctic ABL in sea ice-covered regions has been observed e.g. by Allan et al. (2015); Sipilä et al. (2016); Baccarini et al. (2020); Beck et al. (2021). In these studies, concurrent chemical measurements suggested a link between iodine species and NPF events. Furthermore, it has been shown for both the Arctic and Antarctica that iodine can be emitted from the sea ice. Potential sources include marine microalgae (diatoms) growing below the sea ice (Hill and Manley, 2009; Atkinson et al., 2012), where the iodine can be emitted through cracks and leads and has been connected to thinning Arctic sea ice (Cuevas et al., 2018). The sea ice itself or the snowpack can also release iodine via abiotic, photo-chemical processes (Gálvez et al.,

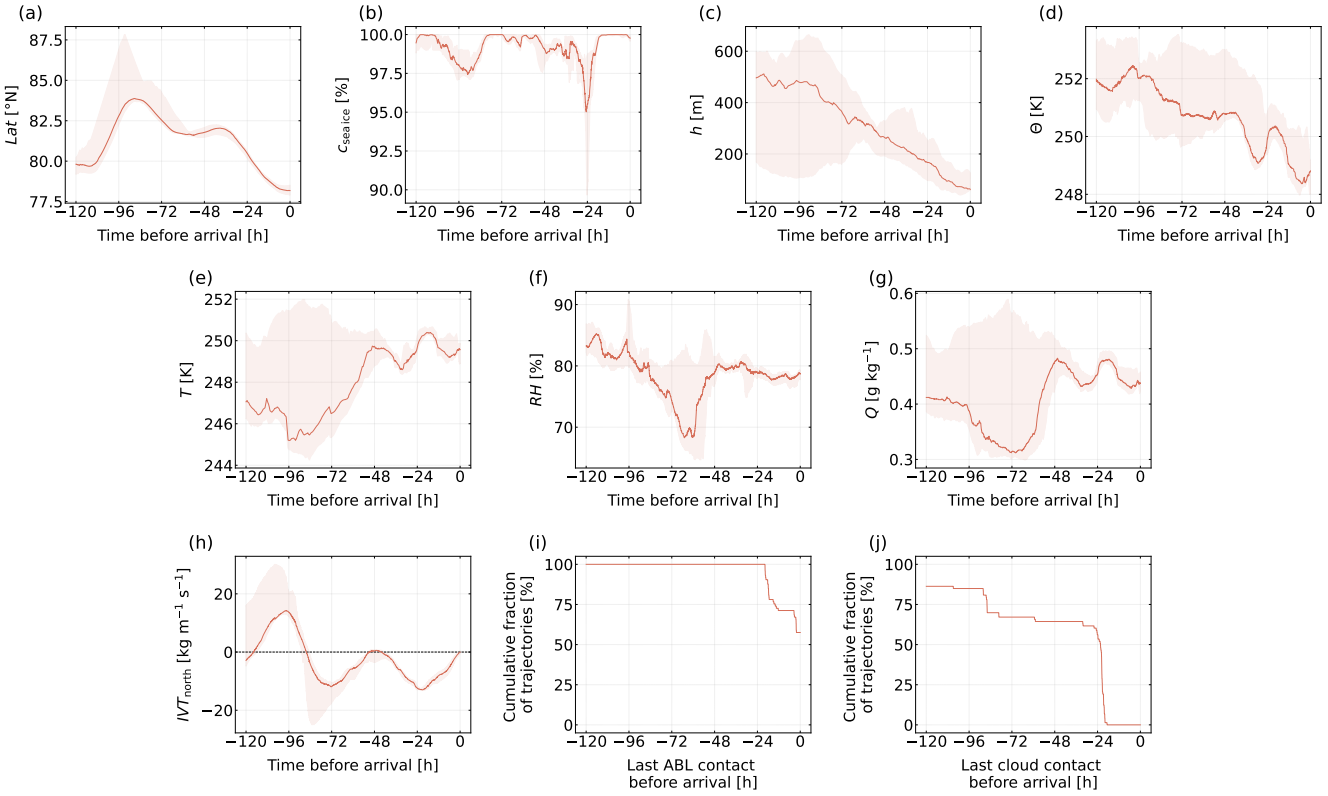


Figure 9. Comparison of geographical and meteorological parameters along the backward trajectories of flight sections linked to newly formed particles inside the ABL over sea ice for the events on 13 and 15 April. Shown, as a function of time prior to arrival, are median values (solid lines) and interquartile ranges (shaded areas) of **(a)** latitude Lat, **(b)** sea ice concentration c_{seaice}, **(c)** altitude h, **(d)** potential temperature Θ, **(e)** absolute temperature T, **(f)** relative humidity RH, **(g)** specific humidity Q, and **(h)** northward integrated water vapor transport IVT_{north}. The last two subplots show the cumulative fraction of the last contact of the trajectories with the **(i)** ABL and **(j)** clouds. Note that if the cumulative fraction does not increase to 100 % at $t = -120\,\text{h}$, this indicates that a fraction of the trajectories was not in contact with the ABL/clouds during the last five days (the maximum time span the calculated trajectories cover).

2016; Kim et al., 2016; Raso et al., 2017). Yet, since we cannot resolve the particle composition of nucleation mode particles nor conducted gas-phase measurements, at this point, we cannot ultimately determine the precursor gases which could have participated in the formation of the newly formed particles observed in this case study. Nevertheless, these previous results suggest the sea ice-covered target area as a plausible source region of precursor gases and newly formed particles.

In summary, from our observations, we hypothesize that the observed presence of newly formed particles in the ABL over sea ice is connected to precursor gases (conceivably iodine components, as reported by Allan et al., 2015; Sipilä et al., 2016; Baccarini et al., 2020; Beck et al., 2021) which originate from natural, most likely regional, but possibly also higher-latitude Arctic sources within the sea ice, from leads, or snow.

3.4 Newly formed particles in the vicinity of clouds

Newly formed particles in the vicinity of clouds were, e.g., encountered on 24 April 2024 during RF08, while flying north of Svalbard over sea ice (open leads and cracks were present, see Fig. S12) with an initially slightly broken and then closed stratocumulus cloud deck (Fig. 10a). Measurements were carried out below cloud base and at cloud top.

On 24 April, a high pressure system was centered directly over Svalbard, resulting in westerly flow in the target region. The air mass probed at altitudes between approximately 600 m and 1200 m originated either in the North Atlantic close to Greenland, near Iceland, or northern Scandinavia (Fig. 10b), and was advected from the North Atlantic marine ABL and lifted above the sea ice, where this layer was decoupled from the surface (Sect. S8.2, Fig. S13). At the top of that elevated mixed layer, stratocumulus clouds were present (Fig. 10a), with a cloud base at about 800 m altitude, and cloud top at about 1150 m. The air mass that was probed at about 2100 m in the free troposphere originated in northern Canada and passed over Greenland on its way to the P6 position (Fig. 10c).

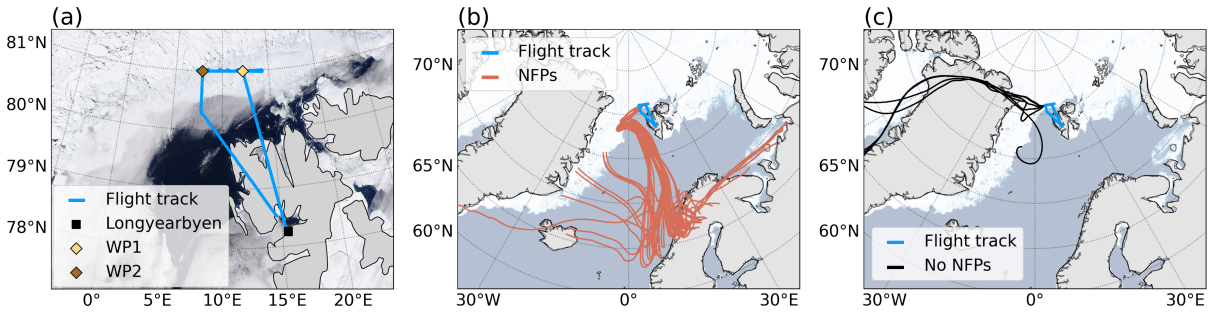


Figure 10. (a) Flight track of RF08 on 24 April 2024. The MODIS-TERRA satellite image was retrieved from https://wvs.earthdata.nasa.gov. **(b)** Five-day backward trajectories associated with newly formed particles (NFPs) along the section of the flight track shown in Fig. 11. **(c)** Five-day backward trajectories connected to PNSD measurements featuring no newly formed particles. The sea ice concentration data shown in the subplots (b) and (c) were retrieved from www.seaice.uni-bremen.de (Spreen et al., 2008).

Here, we specifically discuss the data collected between WP1 and WP2 over a distance of 75 km in the time period between 10:28 and 11:35 UTC. This time period includes a descent from approximately 2100 m down to below cloud level (10:29 to 10:35 UTC), a leg at cloud base (10:35 to 10:52 UTC), an ascent through cloud with subsequent drying away of the ice collected inside cloud, and finally a leg at cloud top (11:07 to 11:35 UTC). With respect to the aerosol particle measurements, the time period from 10:52 to 11:07 UTC, i.e., the ascent through cloud and the subsequent drying away of ice, is excluded from further analysis, as erroneous measurements due to icing of the aerosol inlet and/or droplet shattering (Weber et al., 1998) cannot be ruled out. The MPSS data from this period are grayed out in Fig. 11b, c.

The PNSDs at cloud top and at cloud base featured a pronounced nucleation mode and correspondingly enhanced number concentrations in the nucleation mode size range from 10 nm to 20 nm, regardless of the cloud cover being closed or broken (Fig. 11). In contrast, in the PNSD measured during the descent ~~towards~~ toward cloud level around 10:30 UTC, which we assume to be representative for the free troposphere, concentrations in the sub-20 nm size range were low. This PNSD should be consid-

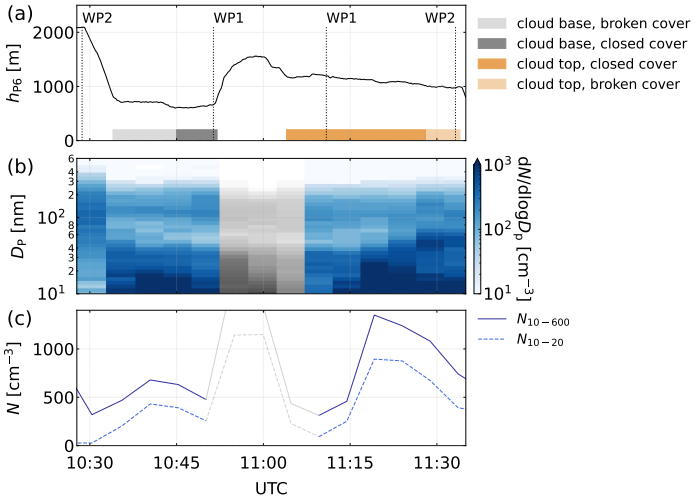


Figure 11. **(a)** P6 altitude during RF08 on 24 April 2024. **(b)** MPSS-measured PNSD. **(c)** Integral particle number concentrations in the total measured size range ($10\ \mathrm{nm} \leq D_\mathrm{p} \leq 600\ \mathrm{nm}$, solid line) and in the nucleation mode size range ($10\ \mathrm{nm} \leq D_\mathrm{p} \leq 20\ \mathrm{nm}$, dashed line), respectively. The data measured from 10:52 to 11:07 UTC are grayed out in panels (b) and (c) since erroneous measurements due to icing of the aerosol inlet and/or droplet shattering cannot be ruled out.

ered semi-quantitative only, as it represents an average over an altitude range of more than 1000 m. The presence/absence of particles in the size range from 10 nm to 20 nm is also clearly visible in Fig. 11c, with particles in the size range below 20 nm contributing approximately 67 %, 60 %, and 9 % to the total aerosol particle number concentrations at cloud top, cloud base, and in the free troposphere, respectively. A more detailed comparison between PNSDs measured at cloud top and at cloud base reveals an interesting effect (Fig. 12). The overall shapes of the distributions are qualitatively similar, with the cloud top and cloud base accumulation mode concentrations following each other rather closely, while the number of Aitken and nucleation mode particles is reduced by roughly a factor of two to three at cloud base, resulting in a more pronounced Hoppel-minimum for the PNSDs measured at cloud base. Even a small shift of the accumulation mode at cloud base to larger sizes can be seen, which could be due to particle growth inside cloud. For the comparison of the PNSDs measured at cloud top and cloud base, we only considered measurements carried out in the exact same geographical area, i.e., measurements between WP1 and WP2 from approximately 10:38 to 10:52 UTC (cloud base) and 11:17 to 11:31 UTC (cloud top). However, as differences are small and spatial and/or temporal variability cannot fully be ruled out, we cannot draw solid quantitative conclusions. To indicate the absence of nucleation mode particles in the free troposphere, the PNSD measured during the descent from 2100 m ~~towards~~ toward cloud level is also shown in Fig. 12.

Backward trajectory analysis of all air masses featuring newly formed particles in the vicinity of clouds

Fig.13 presents the results of the backward trajectory analysis carried out for all PNSD measurements featuring newly formed

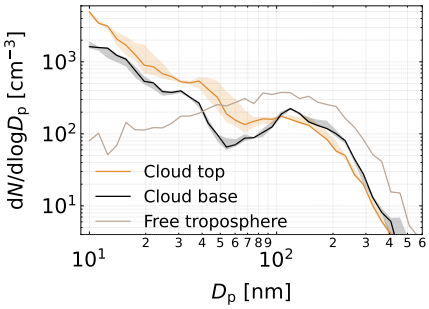


Figure 12. Median PNSDs measured at cloud top, cloud base, and in the free troposphere. The shaded areas represent the interquartile ranges.

particles in the vicinity of clouds, which were observed during three different research flights on 23, 24 (case study), and 26 April.

Predominantly, the air masses approached from lower latitudes and moved northward, mainly in the last 48 hours prior to arrival (Fig. 13a). The trajectories traveled over the open sea in the last 18 to 60 hours and 90 to 100 hours (Fig. 13b), whereby they became warmer and picked up humidity (Fig. 13e-g). Since the moist air masses moved poleward, an increase of IVT_{north} is visible in the last 48 hours before arrival (Fig. 13h). Almost 75 % of the trajectories were in contact with the ABL during the last five days (Fig. 13i), presenting the opportunity for moisture and gaseous precursor uptake, potentially from the open ocean. In about 90 % of the air masses, clouds had formed within the previous five days (Fig. 13j). The gradual decrease in potential temperature found in the last 24 hours prior to arrival (Fig. 13d) ~~may~~ might result from the presence of these clouds, i.e., from cloud top radiative cooling.

Cloud tops, due to the prevailing high humidities and high actinic fluxes, which enhance photochemically driven processes, as well as the presence of potential particle precursors released from evaporating droplets, have been reported to be favorable locations for NPF to take place (e.g., Hegg et al., 1990; Clarke et al., 1998; Weber et al., 2001; Keil and Wendisch, 2001; Wehner et al., 2015). In the Arctic, enhanced concentrations of particles in the size range from 20 nm to 300 nm at the top of stratus clouds were previously observed by Garrett et al. (2002), who suggested that recent particle formation at cloud top lead to these high concentrations. Similarly, a burst of nucleation mode particles within 50 m of the top of an Arctic low-level cloud was recently detected by Pohorsky et al. (2026).

Overall, this leads us to the hypothesis that NPF in the vicinity of the cloud top led to the observed elevated concentrations of newly formed particles at cloud top and cloud base, with the newly formed particles being simultaneously mixed down and cloud processed (wet scavenging and/or growth depending on their size). Such a process is conceivable for a marine ABL with the dynamics of radiatively cooled clouds (radiative cooling rate at cloud top $\approx -120\ \mathrm{K\,d^{-1}}$, Fig. S14, Lonardi et al. (2024)) and the related transport and mixing processes (Wood, 2012). Considering the abundance of Arctic stratiform mixed-phase clouds (e.g., Shupe et al., 2013), NPF in the vicinity of such clouds may play an important role in the Arctic aerosol particle and CCN budgets.

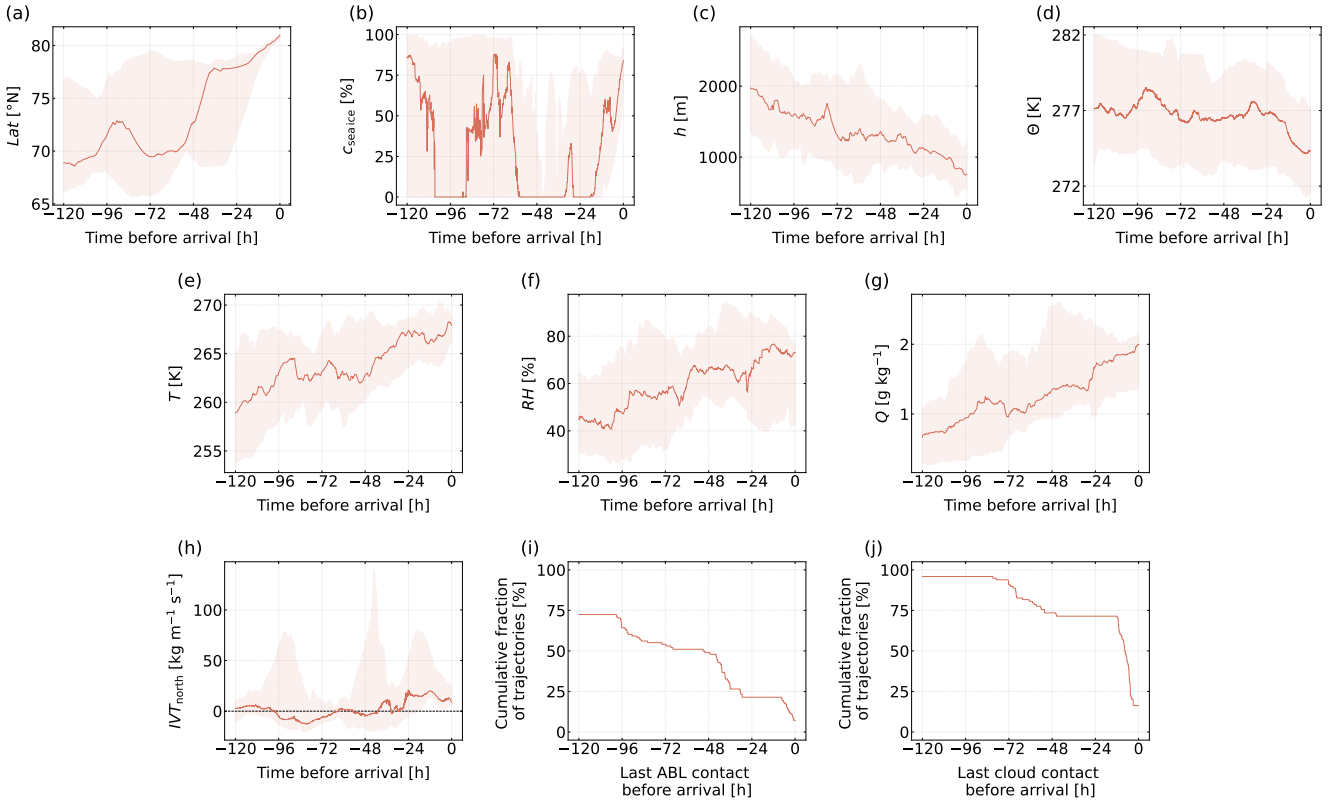


Figure 13. Meteorological parameters along backward trajectories linked to newly formed particles detected in the vicinity of clouds. Shown, as a function of time prior to arrival, are median values (solid lines) and interquartile ranges (shaded areas) of **(a)** latitude Lat, **(b)** sea ice concentration c_{seaice}, **(c)** altitude h, **(d)** potential temperature Θ, **(e)** absolute temperature T, **(f)** relative humidity RH, **(g)** specific humidity Q, and **(h)** northward integrated water vapor transport IVT_{north}. The last two subplots show the cumulative fraction of the last contact of the trajectories with the **(i)** ABL and **(j)** clouds. Note that if the cumulative fraction does not increase to 100 % at $t = -120\,\mathrm{h}$, this indicates that a fraction of the trajectories was not in contact with the ABL/clouds during the last five days (the maximum time span the calculated trajectories cover).

4 Conclusions

In this study, we discussed the frequent occurrence of newly formed aerosol particles in the Arctic troposphere as observed during the airborne measurement campaign BACSAM II, which was conducted from 5 April 2024 to 2 May 2024 utilizing the Alfred Wegener Institute's Polar 6 aircraft (Wesche et al., 2016). The Polar 6 was instrumented with dedicated meteorological and aerosol instrumentation collecting data over and around the Svalbard Archipelago, over the Fram Strait, and in the vicinity of Villum Research Station (Station Nord) in Greenland. We observed newly formed particles during all eleven research flights at various locations (approximately between 76°N to 85°N and 15°W to 26°E). Newly formed particles were encountered in an altitude range from about 60 m to 3900 m above sea level, i.e., throughout the flight altitude range investigated during the

campaign. Specifically, these particles were detected in the free troposphere, inside the atmospheric boundary layer (ABL) over sea ice, in the vicinity of clouds, as well as inside the ABL over ocean with sea ice floes. No clear indications ~~for~~ of newly formed particles inside the ABL over open, completely ice-free ocean were found.

Newly formed particles in the free troposphere were encountered across large geographical areas (with individual events spanning distances of hundreds of kilometers) and at different altitudes. Our respective analyses suggest a possibly important role of meridional transport in combination with cloud processing and precipitation for free tropospheric new particle formation (NPF). Such a scenario could be encountered during, e.g., warm-air intrusions which may deliver the precursor gases to atmospheric conditions (high altitudes, intense solar radiation, low temperatures, small pre-existing particle surface area) favorable for NPF. With respect to the newly formed particles detected inside the ABL over sea ice, we hypothesize that these particles are the result of regional NPF events induced by precursor gases (conceivably iodine components) originating from the sea ice, leads, or snow present in the measurement region. However, contributions of higher-latitude Arctic (precursor) sources cannot be ruled out. Concerning newly formed particles observed at both cloud tops and cloud bases, we found indications that these particles are formed at the cloud tops and subsequently mixed down to the cloud bases, with the cloud tops providing a favorable environment for NPF to occur. The presence of newly formed particles inside the ABL over ocean with sea ice floes could partly be related to a phytoplankton bloom which occurred in the respective target region on the day of the research flight. But ultimately, the source of precursors which ~~could contribute to NPF~~ contributed to the formation of the observed newly formed particles could not be identified. Furthermore, our analysis suggests that during the measurements carried out inside the ABL over open, completely ice-free ocean, no phytoplankton bloom occurred in the target regions, i.e., no indications pointing toward significant emissions of biologically-produced precursors were found. This might explain why no newly formed particles over open ocean were observed during our campaign.

Taken together, our results show that newly formed particles were frequently present and very likely produced in ~~the~~ both the Arctic free troposphere and the Arctic ABL during our measurements in spring 2024. In particular, for the first time, our study presents observational results which indicate that NPF in the Arctic free troposphere occurred over distances of several hundreds of kilometers. In this context, a possible mechanism leading to Arctic free tropospheric NPF could be associated with warm-air intrusions. A similar transport pathway of precursor gases and/or newly formed particles from lower latitudes to the Arctic free troposphere was previously suggested in a modeling study by Price et al. (2023), but to date had not been substantiated by analysis of in situ-measured data. We present observational evidence which likewise shows that meridional transport can lead to NPF in the Arctic free troposphere.

Further modeling studies are required to assess the impact of newly formed particles occurring over distances of hundreds of kilometers and a wide range of altitudes inside and above the Arctic ABL on the Arctic aerosol and cloud condensation nuclei (CCN) budgets. In particular, because relatively small, sub-100 nm particles readily act as CCN in the clean Arctic atmosphere, the occurrence of newly formed particles in the free troposphere and the ABL might exert an important influence on Arctic aerosol-cloud-climate interactions. Future observational campaigns would profit from trace gas measurements and fast, size-resolved measurements of particles with diameters of less than 10 nm, e.g., with multiple condensation particle counters featuring different lower cut-off diameters. Such measurements ~~would~~ could facilitate the identification of the relevant

precursor gases and the precise nucleation region. Importantly, prospective studies should include vertical measurements and target both the Arctic ABL and free troposphere. Here, the use of drop sondes to provide high-resolution profiles of the vertical structure of the atmosphere would be beneficial.

Finally, in a rapidly warming Arctic, where the sea ice continues to retreat, more clouds might be present in the future, and the occurrence of warm-air intrusions is expected to increase, NPF frequency and location will likely be affected by these changes. Especially NPF in the free troposphere, possibly linked to warm-air intrusions, and at the tops of Arctic stratiform clouds, might significantly impact current and future Arctic aerosol and CCN budgets due to its potentially large geographical extent and frequent occurrence, and should therefore be considered in atmospheric models for the prediction of future Arctic weather and climate.

Data availability. Master tracks are available on PANGAEA for all research flights of the BACSAM II campaign (Jurányi et al., 2024). Backward trajectory data are available on PANGAEA for all research flights of the BACSAM II campaign (Kirbus and Wendisch, 2024). PNSD data from all research flights of the BACSAM II campaign are available on PANGAEA (Simon et al., 2026). Sea ice data were retrieved from www.seaice.uni-bremen.de (Spreen et al., 2008). MODIS-TERRA satellite images were retrieved from https://wvs.earthdata.nasa.gov. This study has been conducted using E.U. Copernicus Marine Service Information; https://www.doi.org/10.48670/moi-00281.

Author contributions. DJS participated in the data collection and flight planning during the BACSAM II campaign, analyzed and interpreted the data, and wrote the manuscript. JS participated in the data collection and flight planning, discussed the data, and contributed to the writing. JH participated in the data collection and flight planning, and processed the position, nose boom, and humidity data. BK performed the trajectory calculations and supported their analysis. JM participated in the data collection, flight planning, and calculated the radiative heating/cooling rates. ZJ, MH, BW, LK,AMJ, and MW participated in the flight planning, and the data collection and related discussions. KW was responsible for the development of the MPSS system. AH and ZJ functioned as PIs during the campaign. AH, ZJ, SH, GCR, MW, and MLP contributed to the discussion of the results. FS conceived the study, functioned as PI during the campaign, and contributed to data interpretation and writing. All authors read and edited the manuscript.

Competing interests. The authors declare no competing interests.

Acknowledgements. We gratefully acknowledge the funding by the Deutsche Forschungsgemeinschaft (DFG, German Research Foundation) – Project Number 268020496 – TRR 172, within the framework of the Transregional Collaborative Research Center "ArctiC Amplification: Climate Relevant Atmospheric and SurfaCe Processes, and Feedback Mechanisms (AC)^3", as well as the support of the ~~Alfred-Wegener-Institute~~Alfred Wegener Institute, Helmholtz Centre for Polar and Marine Research through grant number AWI_PA_02172. The authors used ~~a large language model~~ large language models (ChatGPT by OpenAI, Claude by Anthropic) solely to support coding tasks; all scientific reasoning, methodological decisions, analyses, and conclusions were developed independently by the authors.

References

Allan, J. D., Williams, P. I., Najera, J., Whitehead, J. D., Flynn, M. J., Taylor, J. W., Liu, D., Darbyshire, E., Carpenter, L. J., Chance, R., Andrews, S. J., Hackenberg, S. C., and McFiggans, G.: Iodine observed in new particle formation events in the Arctic atmosphere during ACCACIA, Atmospheric Chemistry and Physics, 15, 5599–5609, https://doi.org/10.5194/acp-15-5599-2015, 2015.

Andreae, M. and Rosenfeld, D.: Aerosol–cloud–precipitation interactions. Part 1. The nature and sources of cloud-active aerosols, Earth-Science Reviews, 89, 13–41, https://doi.org/10.1016/j.earscirev.2008.03.001, 2008.

Asmi, E., Kondratyev, V., Brus, D., Laurila, T., Lihavainen, H., Backman, J., Vakkari, V., Aurela, M., Hatakka, J., Viisanen, Y., Uttal, T., Ivakhov, V., and Makshtas, A.: Aerosol size distribution seasonal characteristics measured in Tiksi, Russian Arctic, Atmospheric Chemistry and Physics, 16, 1271–1287, https://doi.org/10.5194/acp-16-1271-2016, 2016.

Atkinson, H. M., Huang, R.-J., Chance, R., Roscoe, H. K., Hughes, C., Davison, B., Schönhardt, A., Mahajan, A. S., Saiz-Lopez, A., Hoffmann, T., and Liss, P. S.: Iodine emissions from the sea ice of the Weddell Sea, Atmospheric Chemistry and Physics, 12, 11 229–11 244, https://doi.org/10.5194/acp-12-11229-2012, 2012.

Baccarini, A., Karlsson, L., Dommen, J., Duplessis, P., Vüllers, J., Brooks, I. M., Saiz-Lopez, A., Salter, M., Tjernström, M., Baltensperger, U., et al.: Frequent new particle formation over the high Arctic pack ice by enhanced iodine emissions, Nature Communications, 11, 4924, https://doi.org/10.1038/s41467-020-18551-0, 2020.

Beck, L. J., Sarnela, N., Junninen, H., Hoppe, C. J., Garmash, O., Bianchi, F., Riva, M., Rose, C., Peräkylä, O., Wimmer, D., et al.: Differing mechanisms of new particle formation at two Arctic sites, Geophysical Research Letters, 48, e2020GL091 334, https://doi.org/10.1029/2020GL091334, 2021.

Bigg, E. K. and Leck, C.: Cloud-active particles over the central Arctic Ocean, Journal of Geophysical Research: Atmospheres, 106, 32 155–32 166, https://doi.org/https://doi.org/10.1029/1999JD901152, 2001.

Bintanja, R., van der Wiel, K., van der Linden, E. C., Reusen, J., Bogerd, L., Krikken, F., and Selten, F. M.: Strong future increases in Arctic precipitation variability linked to poleward moisture transport, Science Advances, 6, eaax6869, https://doi.org/10.1126/sciadv.aax6869, 2020.

Box, J. E., Colgan, W. T., Christensen, T. R., Schmidt, N. M., Lund, M., Parmentier, F.-J. W., Brown, R., Bhatt, U. S., Euskirchen, E. S., Romanovsky, V. E., Walsh, J. E., Overland, J. E., Wang, M., Corell, R. W., Meier, W. N., Wouters, B., Mernild, S., Mård, J., Pawlak, J., and Olsen, M. S.: Key indicators of Arctic climate change: 1971–2017, Environmental Research Letters, 14, 045 010, https://doi.org/10.1088/1748-9326/aafc1b, 2019.

Burkart, J., Willis, M. D., Bozem, H., Thomas, J. L., Law, K., Hoor, P., Aliabadi, A. A., Köllner, F., Schneider, J., Herber, A., et al.: Summertime observations of elevated levels of ultrafine particles in the high Arctic marine boundary layer, Atmospheric Chemistry and Physics, 17, 5515–5535, https://doi.org/10.5194/acp-17-5515-2017, 2017.

Carslaw, K., Lee, L., Reddington, C., Pringle, K., Rap, A., Forster, P., Mann, G., Spracklen, D., Woodhouse, M., Regayre, L., et al.: Large contribution of natural aerosols to uncertainty in indirect forcing, Nature, 503, 67–71, https://doi.org/10.1038/nature12674, 2013.

Clarke, A., Varner, J., Eisele, F., Mauldin, R., Tanner, D., and Litchy, M.: Particle production in the remote marine atmosphere: Cloud outflow and subsidence during ACE 1, Journal of Geophysical Research: Atmospheres, 103, 16 397–16 409, https://doi.org/10.1029/97JD02987, 1998.

Croft, B., Wentworth, G. R., Martin, R. V., Leaitch, W. R., Murphy, J. G., Murphy, B. N., Kodros, J. K., Abbatt, J. P., and Pierce, J. R.: Contribution of Arctic seabird-colony ammonia to atmospheric particles and cloud-albedo radiative effect, Nature Communications, 7, 13 444, https://doi.org/10.1038/ncomms13444, 2016.

Cuevas, C. A., Maffezzoli, N., Corella, J. P., Spolaor, A., Vallelonga, P., Kjær, H. A., Simonsen, M., Winstrup, M., Vinther, B., Horvat, C., et al.: Rapid increase in atmospheric iodine levels in the North Atlantic since the mid-20th century, Nature Communications, 9, 1452, https://doi.org/https://doi.org/10.1038/s41467-018-03756-1, 2018.

Dada, L., Angot, H., Beck, I., Baccarini, A., Quéléver, L. L., Boyer, M., Laurila, T., Brasseur, Z., Jozef, G., De Boer, G., et al.: A central arctic extreme aerosol event triggered by a warm air-mass intrusion, Nature Communications, 13, 5290, https://doi.org/10.1038/s41467-022-32872-2, 2022.

Dall'Osto, M., Beddows, D., Tunved, P., Krejci, R., Ström, J., Hansson, H.-C., Yoon, Y., Park, K.-T., Becagli, S., Udisti, R., et al.: Arctic sea ice melt leads to atmospheric new particle formation, Scientific Reports, 7, 3318, https://doi.org/10.1038/s41598-017-03328-1, 2017.

Dall'Osto, M., Geels, C., Beddows, D., Boertmann, D., Lange, R., Nøjgaard, J., Harrison, R. M., Simo, R., Skov, H., and Massling, A.: Regions of open water and melting sea ice drive new particle formation in North East Greenland, Scientific Reports, 8, 6109, https://doi.org/10.1038/s41598-018-24426-8, 2018.

Engvall, A.-C., Krejci, R., Ström, J., Minikin, A., Treffeisen, R., Stohl, A., and Herber, A.: In-situ airborne observations of the microphysical properties of the Arctic tropospheric aerosol during late spring and summer, Tellus B: Chemical and Physical Meteorology, 60, 392–404, https://doi.org/10.1111/j.1600-0889.2008.00348.x, 2008.

Forster, P., Storelvmo, T., Armour, K., Collins, W., Dufresne, J.-L., Frame, D., Lunt, D. J., Mauritsen, T., Palmer, M. D., Watanabe, M., Wild, M., and Zhang, H.: The Earth's Energy Budget, Climate Feedbacks, and Climate Sensitivity, in: Climate Change 2021: The Physical Science Basis. Contribution of Working Group I to the Sixth Assessment Report of the Intergovernmental Panel on Climate Change, edited by Masson-Delmotte, V., Zhai, P., Pirani, A., Connors, S. L., Péan, C., Berger, S., Caud, N., Chen, Y., Goldfarb, L., Gomis, M. I., Huang, M., Leitzell, K., Lonnoy, E., Matthews, J. B. R., Maycock, T. K., Waterfield, T., Yelekçi, O., Yu, R., and Zhou, B., pp. 923–1054, Cambridge University Press, Cambridge, United Kingdom and New York, NY, USA, https://doi.org/10.1017/9781009157896.009, 2021.

Freud, E., Krejci, R., Tunved, P., Leaitch, R., Nguyen, Q. T., Massling, A., Skov, H., and Barrie, L.: Pan-Arctic aerosol number size distributions: seasonality and transport patterns, Atmospheric Chemistry and Physics, 17, 8101–8128, https://doi.org/10.5194/acp-17-8101-2017, 2017.

Galí, M., Devred, E., Babin, M., and Levasseur, M.: Decadal increase in Arctic dimethylsulfide emission, Proceedings of the National Academy of Sciences, 116, 19 311–19 317, https://doi.org/10.1073/pnas.190437811, 2019.

Gálvez, O., Baeza-Romero, M. T., Sanz, M., and Saiz-Lopez, A.: Photolysis of frozen iodate salts as a source of active iodine in the polar environment, Atmospheric Chemistry and Physics, 16, 12 703–12 713, https://doi.org/10.5194/acp-16-12703-2016, 2016.

Garrett, T. J., Hobbs, P. V., and Radke, L. F.: High Aitken nucleus concentrations above cloud tops in the Arctic, Journal of the Atmospheric Sciences, 59, 779–783, https://doi.org/10.1175/1520-0469(2001)059<0779:HANCAC>2.0.CO;2, 2002.

Gordon, H., Kirkby, J., Baltensperger, U., Bianchi, F., Breitenlechner, M., Curtius, J., Dias, A., Dommen, J., Donahue, N. M., Dunne, E. M., et al.: Causes and importance of new particle formation in the present-day and preindustrial atmospheres, Journal of Geophysical Research: Atmospheres, 122, 8739–8760, https://doi.org/10.1002/2017JD026844, 2017.

Hartmann, J., Gehrmann, M., Kohnert, K., Metzger, S., and Sachs, T.: New calibration procedures for airborne turbulence measurements and accuracy of the methane fluxes during the AirMeth campaigns, Atmospheric Measurement Techniques, 11, 4567–4581, https://doi.org/10.5194/amt-11-4567-2018, 2018.

Hegg, D. A., Radke, L. F., and Hobbs, P. V.: Particle production associated with marine clouds, Journal of Geophysical Research: Atmospheres, 95, 13 917–13 926, https://doi.org/10.1029/JD095iD09p13917, 1990.

Hersbach, H., Bell, B., Berrisford, P., Hirahara, S., Horányi, A., Muñoz-Sabater, J., Nicolas, J., Peubey, C., Radu, R., Schepers, D., et al.: The ERA5 global reanalysis, Quarterly Journal of the Royal Meteorological Society, 146, 1999–2049, https://doi.org/10.1002/qj.3803, 2020.

Heslin-Rees, D., Burgos, M., Hansson, H.-C., Krejci, R., Ström, J., Tunved, P., and Zieger, P.: From a polar to a marine environment: has the changing Arctic led to a shift in aerosol light scattering properties?, Atmospheric Chemistry and Physics, 20, 13 671–13 686, https://doi.org/10.5194/acp-20-13671-2020, 2020.

Hill, V. L. and Manley, S. L.: Release of reactive bromine and iodine from diatoms and its possible role in halogen transfer in polar and tropical oceans, Limnology and Oceanography, 54, 812–822, https://doi.org/10.4319/lo.2009.54.3.0812, 2009.

Igel, A. L., Ekman, A. M., Leck, C., Tjernström, M., Savre, J., and Sedlar, J.: The free troposphere as a potential source of arctic boundary layer aerosol particles, Geophysical Research Letters, 44, 7053–7060, https://doi.org/10.1002/2017GL073808, 2017.

Jurányi, Z., Stratmann, F., Herber, A., Wendisch, M., and Borrmann, S.: Master tracks in different resolutions during POLAR 6 campaign P6-247_BACSAM2_2024, https://doi.org/10.1594/PANGAEA.971763, 2024.

Jurányi, Z., Lüpkes, C., Stratmann, F., Hartmann, J., Schaefer, J., Jörss, A.-M., Schulz, A., Wetzel, B., Simon, D., Gebhard, E., Stöhr, M., Hofmann, P., Kalmbach, D., Grawe, S., Wendisch, M., and Herber, A.: The T-Bird – a new aircraft-towed instrument platform to measure aerosol properties and turbulence close to the surface: introduction to the aerosol measurement system, Atmospheric Measurement Techniques, 18, 3477–3494, https://doi.org/10.5194/amt-18-3477-2025, 2025.

Keil, A. and Wendisch, M.: Bursts of Aitken mode and ultrafine particles observed at the top of continental boundary layer clouds, Journal of Aerosol Science, 32, 649–660, https://doi.org/10.1016/S0021-8502(00)00102-6, 2001.

Kerminen, V.-M., Chen, X., Vakkari, V., Petäjä, T., Kulmala, M., and Bianchi, F.: Atmospheric new particle formation and growth: review of field observations, Environmental Research Letters, 13, 103 003, https://doi.org/10.1088/1748-9326/aadf3c, 2018.

Khadir, T., Riipinen, I., Talvinen, S., Heslin-Rees, D., Pöhlker, C., Rizzo, L., Machado, L. A. T., Franco, M. A., Kremper, L. A., Artaxo, P., Petäjä, T., Kulmala, M., Tunved, P., Ekman, A. M. L., Krejci, R., and Virtanen, A.: Sink, Source or Something In-Between? Net Effects of Precipitation on Aerosol Particle Populations, Geophysical Research Letters, 50, e2023GL104 325, https://doi.org/https://doi.org/10.1029/2023GL104325, e2023GL104325 2023GL104325, 2023.

Khosrawi, F., Ström, J., Minikin, A., and Krejci, R.: Particle formation in the Arctic free troposphere during the ASTAR 2004 campaign: a case study on the influence of vertical motion on the binary homogeneous nucleation of H_2SO_4/H_2O, Atmospheric Chemistry and Physics, 10, 1105–1120, https://doi.org/10.5194/acp-10-1105-2010, 2010.

Kim, K., Yabushita, A., Okumura, M., Saiz-Lopez, A., Cuevas, C. A., Blaszczak-Boxe, C. S., Min, D. W., Yoon, H.-I., and Choi, W.: Production of molecular iodine and tri-iodide in the frozen solution of iodide: implication for polar atmosphere, Environmental Science & Technology, 50, 1280–1287, https://doi.org/10.1021/acs.est.5b05148, 2016.

Kirbus, B. and Wendisch, M.: Five-day backwards trajectories at one minute resolution along the flight tracks of the Polar 6 research aircraft during BACSAM II, https://doi.org/10.1594/PANGAEA.971694, 2024.

Kulmala, M. and Kerminen, V.-M.: On the formation and growth of atmospheric nanoparticles, Atmospheric Research, 90, 132–150, https://doi.org/10.1016/j.atmosres.2008.01.005, 2008.

Kulmala, M., Vehkamäki, H., Petäjä, T., Dal Maso, M., Lauri, A., Kerminen, V.-M., Birmili, W., and McMurry, P.: Formation and growth rates of ultrafine atmospheric particles: a review of observations, Journal of Aerosol Science, 35, 143–176, https://doi.org/10.1016/j.jaerosci.2003.10.003, 2004.

Kupiszewski, P., Leck, C., Tjernström, M., Sjogren, S., Sedlar, J., Graus, M., Müller, M., Brooks, B., Swietlicki, E., Norris, S., et al.: Vertical profiling of aerosol particles and trace gases over the central Arctic Ocean during summer, Atmospheric Chemistry and Physics, 13, 12 405–12 431, https://doi.org/10.5194/acp-13-12405-2013, 2013.

Leaitch, W. R., Sharma, S., Huang, L., Toom-Sauntry, D., Chivulescu, A., Macdonald, A. M., von Salzen, K., Pierce, J. R., Bertram, A. K., Schroder, J. C., et al.: Dimethyl sulfide control of the clean summertime Arctic aerosol and cloud, Elementa, 1, 000 017, https://doi.org/10.12952/journal.elementa.000017, 2013.

Leck, C. and Bigg, E. K.: Aerosol production over remote marine areas-A new route, Geophysical Research Letters, 26, 3577–3580, https://doi.org/https://doi.org/10.1029/1999GL010807, 1999.

Lee, S.-H., Gordon, H., Yu, H., Lehtipalo, K., Haley, R., Li, Y., and Zhang, R.: New particle formation in the atmosphere: From molecular clusters to global climate, Journal of Geophysical Research: Atmospheres, 124, 7098–7146, https://doi.org/10.1029/2018JD029356, 2019.

Lonardi, M., Akansu, E. F., Ehrlich, A., Mazzola, M., Pilz, C., Shupe, M. D., Siebert, H., and Wendisch, M.: Tethered balloon-borne observations of thermal-infrared irradiance and cooling rate profiles in the Arctic atmospheric boundary layer, Atmospheric Chemistry and Physics, 24, 1961–1978, https://doi.org/10.5194/acp-24-1961-2024, 2024.

Mauritsen, T., Sedlar, J., Tjernström, M., Leck, C., Martin, M., Shupe, M., Sjogren, S., Sierau, B., Persson, P. O. G., Brooks, I. M., and Swietlicki, E.: An Arctic CCN-limited cloud-aerosol regime, Atmospheric Chemistry and Physics, 11, 165–173, https://doi.org/10.5194/acp-11-165-2011, 2011.

McFarquhar, G. M. and Cober, S. G.: Single-scattering properties of mixed-phase Arctic clouds at solar wavelengths: Impacts on radiative transfer, Journal of Climate, 17, 3799–3813, https://doi.org/10.1175/1520-0442(2004)017<3799:SPOMAC>2.0.CO;2, 2004.

Merikanto, J., Spracklen, D., Mann, G., Pickering, S., and Carslaw, K.: Impact of nucleation on global CCN, Atmospheric Chemistry and Physics, 9, 8601–8616, https://doi.org/10.5194/acp-9-8601-2009, 2009.

Moser, M., Voigt, C., Jurkat-Witschas, T., Hahn, V., Mioche, G., Jourdan, O., Dupuy, R., Gourbeyre, C., Schwarzenboeck, A., Lucke, J., Boose, Y., Mech, M., Borrmann, S., Ehrlich, A., Herber, A., Lüpkes, C., and Wendisch, M.: Microphysical and thermodynamic phase analyses of Arctic low-level clouds measured above the sea ice and the open ocean in spring and summer, Atmospheric Chemistry and Physics, 23, 7257–7280, https://doi.org/10.5194/acp-23-7257-2023, 2023.

Perry, K. D. and Hobbs, P. V.: Further evidence for particle nucleation in clear air adjacent to marine cumulus clouds, Journal of Geophysical Research: Atmospheres, 99, 22 803–22 818, https://doi.org/10.1029/94JD01926, 1994.

Pierce, J. and Adams, P.: Uncertainty in global CCN concentrations from uncertain aerosol nucleation and primary emission rates, Atmospheric Chemistry and Physics, 9, 1339–1356, https://doi.org/10.5194/acp-9-1339-2009., 2009.

Pilz, C., Cassano, J. J., de Boer, G., Kirbus, B., Lonardi, M., Pöhlker, M., Shupe, M. D., Siebert, H., Wendisch, M., and Wehner, B.: Tethered balloon measurements reveal enhanced aerosol occurrence aloft interacting with Arctic low-level clouds, Elementa: Science of the Anthropocene, 12, https://doi.org/10.1525/elementa.2023.00120, 2024.

Pohorsky, R., Guy, H., Brooks, I. M., Haberstock, L., Fauré, N., Zieger, P., Kojoj, J., Murto, S., Calmer, R., Heutte, B., Lonardi, M., Thomson, E. S., Tjernström, M., Creamean, J., Nenes, A., and Schmale, J.: Contribution of free tropospheric aerosols to Arctic low-level cloud droplets formation and longwave radiative forcing, Atmospheric Chemistry and Physics, 26, 10 331–10 353, https://doi.org/10.5194/acp-26-10331-2026, 2026.

Price, R., Baccarini, A., Schmale, J., Zieger, P., Brooks, I. M., Field, P., and Carslaw, K. S.: Late summer transition from a free-tropospheric to boundary layer source of Aitken mode aerosol in the high Arctic, Atmospheric Chemistry and Physics, 23, 2927–2961, https://doi.org/10.5194/acp-23-2927-2023, 2023.

Pruppacher, H. R. and Klett, J. D.: Microphysics of clouds and precipitation, https://doi.org/doi.org/10.1007/978-0-306-48100-0, 2010.

Raso, A. R. W., Custard, K. D., May, N. W., Tanner, D., Newburn, M. K., Walker, L., Moore, R. J., Huey, L. G., Alexander, L., Shepson, P. B., and Pratt, K. A.: Active molecular iodine photochemistry in the Arctic, Proceedings of the National Academy of Sciences, 114, 10 053–10 058, https://doi.org/10.1073/pnas.1702803114, 2017.

Schmale, J. and Baccarini, A.: Progress in unraveling atmospheric new particle formation and growth across the Arctic, Geophysical Research Letters, 48, e2021GL094 198, https://doi.org/10.1029/2021GL094198, 2021.

Schmale, J., Zieger, P., and Ekman, A. M.: Aerosols in current and future Arctic climate, Nature Climate Change, 11, 95–105, https://doi.org/10.1038/s41558-020-00969-5, 2021.

Seinfeld, J. H. and Pandis, S. N.: Atmospheric chemistry and physics: from air pollution to climate change, John Wiley & Sons, 2006.

Serreze, M. C. and Barry, R. G.: Processes and impacts of Arctic amplification: A research synthesis, Global and Planetary Change, 77, 85–96, https://doi.org/10.1016/j.gloplacha.2011.03.004, 2011.

Serreze, M. C. and Francis, J. A.: The Arctic amplification debate, Climatic Change, 76, 241–264, https://doi.org/10.1007/s10584-005-9017-y, 2006.

Shupe, M., Persson, P., Brooks, I., Tjernström, M., Sedlar, J., Mauritsen, T., Sjogren, S., and Leck, C.: Cloud and boundary layer interactions over the Arctic sea ice in late summer, Atmospheric Chemistry and Physics, 13, 9379–9399, https://doi.org/10.5194/acp-13-9379-2013, 2013.

Simon, D. J., Schaefer, J., Hartmann, M., Weinhold, K., and Stratmann, F.: Airborne in-situ measurements of aerosol particle number size distributions during the BACSAM II campaign in April 2024, https://doi.org/10.1594/PANGAEA.993546, 2026.

Sipilä, M., Sarnela, N., Jokinen, T., Henschel, H., Junninen, H., Kontkanen, J., Richters, S., Kangasluoma, J., Franchin, A., Peräkylä, O., et al.: Molecular-scale evidence of aerosol particle formation via sequential addition of HIO3, Nature, 537, 532–534, https://doi.org/10.1038/nature19314, 2016.

Spreen, G., Kaleschke, L., and Heygster, G.: Sea ice remote sensing using AMSR-E 89-GHz channels, Journal of Geophysical Research: Oceans, 113, https://doi.org/10.1029/2005JC003384, 2008.

Sprenger, M. and Wernli, H.: The LAGRANTO Lagrangian analysis tool – version 2.0, Geoscientific Model Development, 8, 2569–2586, https://doi.org/10.5194/gmd-8-2569-2015, 2015.

Stroeve, J., Holland, M. M., Meier, W., Scambos, T., and Serreze, M.: Arctic sea ice decline: Faster than forecast, Geophysical research letters, 34, https://doi.org/10.1029/2007GL029703, 2007.

Von der Weiden, S.-L., Drewnick, F., and Borrmann, S.: Particle Loss Calculator–a new software tool for the assessment of the performance of aerosol inlet systems, Atmospheric Measurement Techniques, 2, 479–494, https://doi.org/10.5194/amt-2-479-2009, 2009.

Wallace, J. M. and Hobbs, P. V.: Atmospheric Science: An Introductory Survey, vol. 92 of *International Geophysics Series*, Elsevier Academic Press, Amsterdam; Boston, 2nd edn., ISBN 978-0-12-732951-2, 2006.

Weber, R., Clarke, A., Litchy, M., Li, J., Kok, G., Schillawski, R., and McMurry, P.: Spurious aerosol measurements when sampling from aircraft in the vicinity of clouds, Journal of Geophysical Research: Atmospheres, 103, 28 337–28 346, https://doi.org/10.1029/98JD02086, 1998.

Weber, R., Chen, G., Davis, D., Mauldin III, R., Tanner, D., Eisele, F., Clarke, A., Thornton, D., and Bandy, A.: Measurements of enhanced H_2SO_4 and 3–4 nm particles near a frontal cloud during the First Aerosol Characterization Experiment (ACE 1), Journal of Geophysical Research: Atmospheres, 106, 24 107–24 117, https://doi.org/10.1029/2000JD000109, 2001.

Weber, R., Orsini, D., Wang, B., Scheuer, E., Talbot, R., Dibb, J. E., Seid, G., DeBell, L., Mauldin, R., Kosciuch, E., et al.: Investigations into free tropospheric new particle formation in the central Canadian arctic during the winter/spring transition as part of TOPSE, Journal of Geophysical Research: Atmospheres, 108, https://doi.org/10.1029/2002JD002239, 2003.

Wehner, B., Werner, F., Ditas, F., Shaw, R. A., Kulmala, M., and Siebert, H.: Observations of new particle formation in enhanced UV irradiance zones near cumulus clouds, Atmospheric Chemistry and Physics, 15, 11 701–11 711, https://doi.org/10.5194/acp-15-11701-2015, 2015.

Wendisch, M., Brückner, M., Burrows, J., Crewell, S., Dethloff, K., Ebell, K., Lüpkes, C., Macke, A., Notholt, J., Quaas, J., et al.: Understanding causes and effects of rapid warming in the Arctic, Eos, https://doi.org/10.1029/2017EO064803, 2017.

Wendisch, M., Brückner, M., Crewell, S., Ehrlich, A., Notholt, J., Lüpkes, C., Macke, A., Burrows, J., Rinke, A., Quaas, J., et al.: Atmospheric and surface processes, and feedback mechanisms determining Arctic amplification: A review of first results and prospects of the $(\mathcal{AC})^3$ project, Bulletin of the American Meteorological Society, 104, E208–E242, https://doi.org/10.1175/BAMS-D-21-0218.1, 2023.

Wendisch, M., Crewell, S., Ehrlich, A., Herber, A., Kirbus, B., Lüpkes, C., Mech, M., Abel, S. J., Akansu, E. F., Ament, F., Aubry, C., Becker, S., Borrmann, S., Bozem, H., Brückner, M., Clemen, H.-C., Dahlke, S., Dekoutsidis, G., Delanoë, J., De La Torre Castro, E., Dorff, H., Dupuy, R., Eppers, O., Ewald, F., George, G., Gorodetskaya, I. V., Grawe, S., Groß, S., Hartmann, J., Henning, S., Hirsch, L., Jäkel, E., Joppe, P., Jourdan, O., Jurányi, Z., Karalis, M., Kellermann, M., Klingebiel, M., Lonardi, M., Lucke, J., Luebke, A. E., Maahn, M., Maherndl, N., Maturilli, M., Mayer, B., Mayer, J., Mertes, S., Michaelis, J., Michalkov, M., Mioche, G., Moser, M., Müller, H., Neggers, R., Ori, D., Paul, D., Paulus, F. M., Pilz, C., Pithan, F., Pöhlker, M., Pörtge, V., Ringel, M., Risse, N., Roberts, G. C., Rosenburg, S., Röttenbacher, J., Rückert, J., Schäfer, M., Schaefer, J., Schemann, V., Schirmacher, I., Schmidt, J., Schmidt, S., Schneider, J., Schnitt, S., Schwarz, A., Siebert, H., Sodemann, H., Sperzel, T., Spreen, G., Stevens, B., Stratmann, F., Svensson, G., Tatzelt, C., Tuch, T., Vihma, T., Voigt, C., Volkmer, L., Walbröl, A., Weber, A., Wehner, B., Wetzel, B., Wirth, M., and Zinner, T.: Overview: quasi-Lagrangian observations of Arctic air mass transformations – introduction and initial results of the HALO–$(\mathcal{AC})^3$ aircraft campaign, Atmospheric Chemistry and Physics, 24, 8865–8892, https://doi.org/10.5194/acp-24-8865-2024, 2024.

Wendisch, M., Kirbus, B., Ori, D., Shupe, M. D., Crewell, S., Sodemann, H., and Schemann, V.: Observed and modeled Arctic air-mass transformations during warm air intrusions and cold air outbreaks, Atmospheric Chemistry and Physics, 25, 15 047–15 076, https://doi.org/10.5194/acp-25-15047-2025, 2025.

Wesche, C., Steinhage, D., and Nixdorf, U.: Polar aircraft Polar5 and Polar6 operated by the Alfred Wegener institute, Journal of Large-Scale Research Facilities, 2, A87–A87, https://doi.org/10.17815/jlsrf-2-153, 2016.

Wiedensohler, A., Covert, D. S., Swietlicki, E., Aalto, P., Heintzenberg, J., and Leck, C.: Occurrence of an ultrafine particle mode less than 20 nm in diameter in the marine boundary layer during Arctic summer and autumn, Tellus B, 48, 213–222, https://doi.org/10.3402/tellusb.v48i2.15887, 1996.

Wiedensohler, A., Birmili, W., Nowak, A., Sonntag, A., Weinhold, K., Merkel, M., Wehner, B., Tuch, T., Pfeifer, S., Fiebig, M., Fjäraa, A. M., Asmi, E., Sellegri, K., Depuy, R., Venzac, H., Villani, P., Laj, P., Aalto, P., Ogren, J. A., Swietlicki, E., Williams, P., Roldin, P., Quincey, P., Hüglin, C., Fierz-Schmidhauser, R., Gysel, M., Weingartner, E., Riccobono, F., Santos, S., Grüning, C., Faloon, K., Beddows, D., Harrison, R., Monahan, C., Jennings, S. G., O'Dowd, C. D., Marinoni, A., Horn, H.-G., Keck, L., Jiang, J., Scheckman, J., McMurry, P. H., Deng, Z., Zhao, C. S., Moerman, M., Henzing, B., de Leeuw, G., Löschau, G., and Bastian, S.: Mobility particle size spectrometers: harmonization of technical standards and data structure to facilitate high quality long-term observations of atmospheric particle number size distributions, Atmospheric Measurement Techniques, 5, 657–685, https://doi.org/10.5194/amt-5-657-2012, 2012.

Wiedensohler, A., Wiesner, A., Weinhold, K., Birmili, W., Hermann, M., Merkel, M., Müller, T., Pfeifer, S., Schmidt, A., Tuch, T., et al.: Mobility particle size spectrometers: Calibration procedures and measurement uncertainties, Aerosol Science and Technology, 52, 146–164, https://doi.org/10.1080/02786826.2017.1387229, 2018.

Willis, M. D., Burkart, J., Thomas, J. L., Köllner, F., Schneider, J., Bozem, H., Hoor, P. M., Aliabadi, A. A., Schulz, H., Herber, A. B., Leaitch, W. R., and Abbatt, J. P. D.: Growth of nucleation mode particles in the summertime Arctic: a case study, Atmospheric Chemistry and Physics, 16, 7663–7679, https://doi.org/10.5194/acp-16-7663-2016, 2016.

Willis, M. D., Köllner, F., Burkart, J., Bozem, H., Thomas, J. L., Schneider, J., Aliabadi, A. A., Hoor, P. M., Schulz, H., Herber, A. B., et al.: Evidence for marine biogenic influence on summertime Arctic aerosol, Geophysical Research Letters, 44, 6460–6470, https://doi.org/10.1002/2017GL073359, 2017.

Willis, M. D., Leaitch, W. R., and Abbatt, J. P.: Processes controlling the composition and abundance of Arctic aerosol, Reviews of Geophysics, 56, 621–671, https://doi.org/10.1029/2018RG000602, 2018.

Wood, R.: Stratocumulus clouds, Monthly Weather Review, 140, 2373–2423, https://doi.org/10.1175/MWR-D-11-00121.1, 2012.

Supporting information to "Frequent occurrence of newly formed aerosol particles over wide geographical areas in the Arctic free troposphere and atmospheric boundary layer"

David J. Simon[1], Jonas Schaefer[1], Jörg Hartmann[2], Benjamin Kirbus[3], Joshua Müller[3], Markus Hartmann[1], Bruno Wetzel[1], Laura Köhler[2], Anna-Marie Jörss[2], Kay Weinhold[1], Andreas Herber[2], Zsófia Jurányi[2], Silvia Henning[1], Gregory C. Roberts[4], Manfred Wendisch[3], Mira L. Pöhlker[1,3], and Frank Stratmann[1]

[1]Atmospheric Microphysics Department, Leibniz Institute for Tropospheric Research, Leipzig, Germany
[2]Alfred Wegener Institute, Helmholtz Centre for Polar and Marine Research, Bremerhaven, Germany
[3]Leipzig Institute for Meteorology, Leipzig University, Leipzig, Germany
[4]Scripps Institution of Oceanography, La Jolla, CA, USA

Correspondence: David J. Simon (simon@tropos.de)

S1 Research flights during the aircraft measurement campaign

Fig. S1 shows the flight tracks of all eleven research flights (RFs) conducted with the Polar 6 (P6) aircraft during the measurement campaign "Boundary layer and Aerosol and Cloud Study in the Arctic, based on aircraft and T-Bird Measurements II" (BACSAM II).

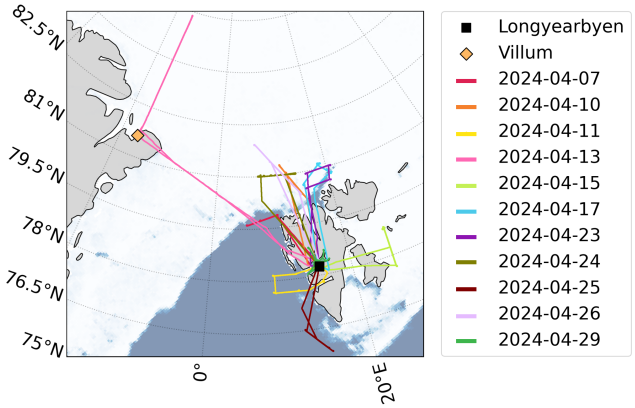


Figure S1. Flight tracks of all research flights during BACSAM II. The sea ice concentration is shown exemplary for 15 April 2024. The corresponding sea ice data were retrieved from www.seaice.uni-bremen.de (Spreen et al., 2008).

S2 Correction for particle losses

To characterize particle losses in the sampling line from the aerosol inlet of the Polar 6 aircraft to the mobility particle size spectrometer (MPSS), we calculated the transmission efficiencies ($\eta = \eta(D_\mathrm{p})$, where D_p is the particle diameter) in the tubing utilizing the Particle Loss Calculator (Von der Weiden et al., 2009). The particle loss calculator includes losses due to diffusion, sedimentation, turbulent inertial deposition, and inertial deposition in bends and contractions. To approximate the aerosol particles' parameters, we assumed a density of $1.77\,\mathrm{g\,cm^{-3}}$, representing the density of ammonium sulfate particles, and a shape factor of 1, corresponding to spherical particles (Seinfeld and Pandis, 2006). As discussed in Sect. 2.2 of the main text, the flow in the sampling tubing is manually adjusted depending on the true airspeed of the aircraft (typically $tas \approx 60\ \mathrm{m\,s^{-1}}$ during flight section at low altitudes in the target regions, and $tas \approx 90\ \mathrm{m\,s^{-1}}$ during flight sections at high altitudes, e.g., transit flights). This procedure enables near-isokinetic sampling (Jurányi et al., 2025). Based on the corresponding flow recordings as well as pressure and temperature measurements of the MPSS throughout the campaign, for the loss calculations, pressure and temperature in the sampling line are set to the respective median values for measurements at high and low altitudes: $p_\mathrm{med} = 761\,\mathrm{hPa}$, $T_\mathrm{med} = 290\,\mathrm{K}$ for $tas \approx 90\ \mathrm{m\,s^{-1}}$, and $p_\mathrm{med} = 987\,\mathrm{hPa}$, $T_\mathrm{med} = 298\,\mathrm{K}$ for $tas \approx 60\ \mathrm{m\,s^{-1}}$. The calculations yield the transmission efficiency curves shown as solid lines in Fig. S2. To estimate the uncertainty in the transmission efficiencies associated with the median settings, we show the transmission efficiencies calculated for the 10th and 90th percentiles of the pressure and temperature distributions as shaded areas in Fig. S2 as well. Here, the respective parameters are set to $p_{10} = 678\,\mathrm{hPa}$, $T_{10} = 286\,\mathrm{K}$, $p_{90} = 905\,\mathrm{hPa}$, $T_{90} = 296\,\mathrm{K}$ for $tas \approx 90\ \mathrm{m\,s^{-1}}$, and $p_{10} = 862\,\mathrm{hPa}$, $T_{10} = 293\,\mathrm{K}$, $p_{90} = 1030\,\mathrm{hPa}$, $T_\mathrm{med} = 300\,\mathrm{K}$ for $tas \approx 60\ \mathrm{m\,s^{-1}}$.

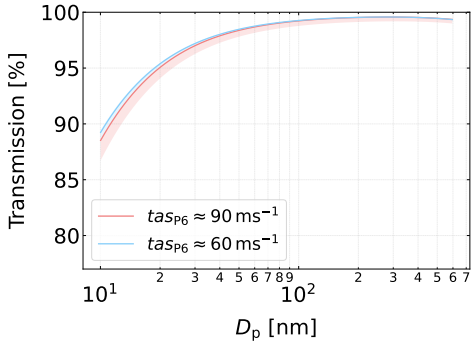


Figure S2. Particle size-dependent transmission efficiencies in the sampling tubing from the aerosol inlet to the MPSS for the two typical true airspeeds of the Polar 6 aircraft during the campaign.

For both typical true airspeeds of the aircraft, the transmission efficiencies calculated for the median pressure and temperature values range from $\approx 89\,\%$ at 10 nm over $\approx 95\,\%$ at 20 nm to $> 99\,\%$ at 100 nm (solid lines in Fig. S2). The values decrease towards smaller particle diameters to their minimum values at 10 nm as diffusional losses increase with decreasing particle size (Baron and Willeke, 2001, Fig. S2). Accordingly, we correct the MPSS-measured particle number size distribution (PNSD) data for particles losses in the sampling tubing by size-dependent correction factors ($c(D_\mathrm{p}) = 1/\eta(D_\mathrm{p})$) ranging from close

to 1 to 1.12. Considering the transmission efficiencies calculated for the 10th and 90th percentiles, maximum differences are $\approx 1\,\%$ for $tas \approx 60\ \mathrm{ms}^{-1}$ and $\approx 2\,\%$ for $tas \approx 90\ \mathrm{ms}^{-1}$ compared to the corrections based on the medians of the pressure and temperature distributions. We consider these errors to be negligible and apply the correction factors based on the median values to all PNSD data.

S3 Atmospheric conditions along the aircraft's flight track

Due to the lack of, e.g., drop sonde and cloud microphysical measurements, ~~we do not have available continuous~~ data concerning the atmospheric stratification and the occurrence of clouds along the flight tracks are not continuously available. In other words, we cannot always unambiguously distinguish the airplane's ~~actual~~ position being within our outside the atmospheric boundary layer (ABL). Furthermore, we cannot always verify the presence or absence of clouds in the aircraft's proximity. However, we can provide a very rough estimate of the total measurement times inside the (cloud-free) ABL, in the (cloud-free) free troposphere~~(FT)~~, and in cloud vicinity based on reanalysis data from the fifth generation ECMWF reanalysis (ERA5) dataset. Thereto, we interpolated several ERA5 parameters such as specific cloud liquid water content ($CLWC$), specific cloud ice water content ($CIWC$), and the ABL height on to the flight track of the Polar 6 aircraft. Here, we consider a flight section to have been carried out in the vicinity of clouds if the sum of $CLWC$ and $CIWC$, i.e., the total cloud water content (~~CWC~~$CWC = CLWC + CIWC$) exceeds the threshold of $CWC > 0.01\,\mathrm{g\,kg}^{-1}$. The latter is based on in situ measurements of CWC of Arctic clouds conducted by McFarquhar and Cober (2004) in April 1998 and Moser et al. (2023) in April 2019. In both studies, values on the order of $CWC \sim 0.01\,\mathrm{g\,kg}^{-1}$ were reported for in-cloud measurements. We consider measurements to have taken place in the free troposphere (ABL) if the aircraft's flight altitude was above (below) the ERA5 ABL height. Here, the flight sections in cloud vicinity based on the threshold above are additionally excluded.

Based on the reanalysis data, for our campaign, we determine a total measurement time of about 25 hours and 10 minutes in the free troposphere, approximately 2 hours and 10 minutes in the vicinity of clouds, and about 8 hours and 10 minutes inside the ABL~~(Table ??)~~. Here, 60 minutes were carried out inside the ABL over ocean with sea ice floes, 3 hours and 30 minutes inside the ABL over sea ice, and 2 hours inside the ABL over open, completely ice-free ocean. In this analysis, the research flight on 29 April was omitted since it was carried out inside the fjords close to Longyearbyen under a completely closed cloud deck. These measurements amount to a duration of 1 hour and 40 minutes. Observations of newly formed particles on this day ($\approx$ 10 minutes) are assigned to the unclassified category.

~~In addition, the relative frequencies of occurrence of newly formed particles for each environment are provided in Table ??. These values should be interpreted carefully and only provide a very rough estimate.~~ The values reported above are associated with rather large uncertainties as they are are not well suited to describe the prevailing conditions at the aircraft's exact position. For example, not for all flight sections dedicated to probe directly the cloud top or cloud base, i.e., legs which are known to have taken place in the direct vicinity of clouds, ERA5 predicted consistently non-zero values of CWC throughout the leg. Furthermore, during the case study on newly formed particles over sea ice, the ERA5-based ABL height was roughly 100 m lower than the ABL height determined from the vertical profiles of potential temperature derived from in situ measurements in

the target region.

For ~~all case studies and the assignment~~ the classification of measurement periods featuring newly formed particles to the ~~four~~ categories "free troposphere", "cloud vicinity", "ABL over sea ice", and "ABL over ocean with sea ice floes", ~~we only consider flight sections~~ including all case studies, we only considered measurements for which the prevailing conditions could be ~~clearly identified~~ unequivocally determined based on the in situ data. If newly formed particles were detected but ~~either, e.g.,~~ the conditions could not unambiguously be identified (e.g., because the ABL height could not be determined for the target region~~or the the~~ , or because the absence/presence of clouds close to the aircraft could not be verified by studying in situ video ~~data~~and radiation data), these observations are assigned to the unclassified cases.

~~Overview of total measurement time as well as duration and frequency of newly formed particle-occurrence (NFP-occurrence) for the four environments. FT ABL ABL ABL over ocean cloud vicinity irrespective of surface over sea ice with sea ice floes Total measurement time 25 h 10 min 8 h 10 min 3 h 30 min 1 h 2 h 10 min(based on ERA5) Duration of NFP-occurrence 4 h 40 min 2 h 20 min 1 h 40 min 40 min 2 h 40 min(based on in situ data) Frequency of NFP-occurrence 19 % 29 % 48 % 67 % (> 100 %)~~

S4 Thermodynamic conditions during the occurrence of newly formed particles

In Fig. S3, relative frequencies of occurrence of measured temperature and relative humidity pairs (T-RH pairs) are plotted in a temperature vs. relative humidity plane. The relative frequencies were computed considering the number of measured T-RH pairs during the presence of newly formed particles (Fig. S3a, 3686703 pairs) and considering the number of T-RH pairs measured during the absence of newly formed particle (Fig. S3b, 9094434 pairs). The histograms shown in Fig. S3c-f were calculated by including the T-RH data pairs recorded only during observations of newly formed particles in the free troposphere (Fig. S3c), only during observations of newly formed particles in the ABL over sea ice (Fig. S3d), only during observations of newly formed particles in the vicinity of clouds (Fig. S3e), and only during observations of newly formed particles in the ABL over ocean with sea ice floes (Fig. S3f). These data are then normalized by the data recorded during all observations of newly formed particles combined. That is, the normalization is the same as for the histogram depicted in Fig. S3a. The dotted horizontal and vertical lines separating the subplot into four quadrants in Fig. S3 are plotted to guide the eyes.

From Fig. S3, a clear pattern becomes visible. The data show three main clusters in the relative frequency distribution of temperature and humidity conditions during observations of newly formed particles (Fig. S3a), while the frequency distribution of T-RH pairs measured during the absence of newly formed particles is broader, with fewer pronounced features (Fig. S3b). The peaks in Fig. S3a, i.e., in the T-RH distribution measured during observations of newly formed particles, correspond to the different environmental scenarios under which newly formed particles were detected. Newly formed particles in the free troposphere were predominantly associated with cold and dry conditions (lower left quadrant in Fig. S3a, Fig. S3c). Newly formed particles in the ABL over sea ice occurred during cold and humid conditions (lower right quadrant in Fig. S3a, Fig. S3d). For newly formed particles detected in the vicinity of clouds, relatively warm and humid conditions prevailed (upper right quadrant in Fig. S3a, Fig. S3e). Similarly, newly formed particles inside the ABL over ocean with sea ice floes occurred

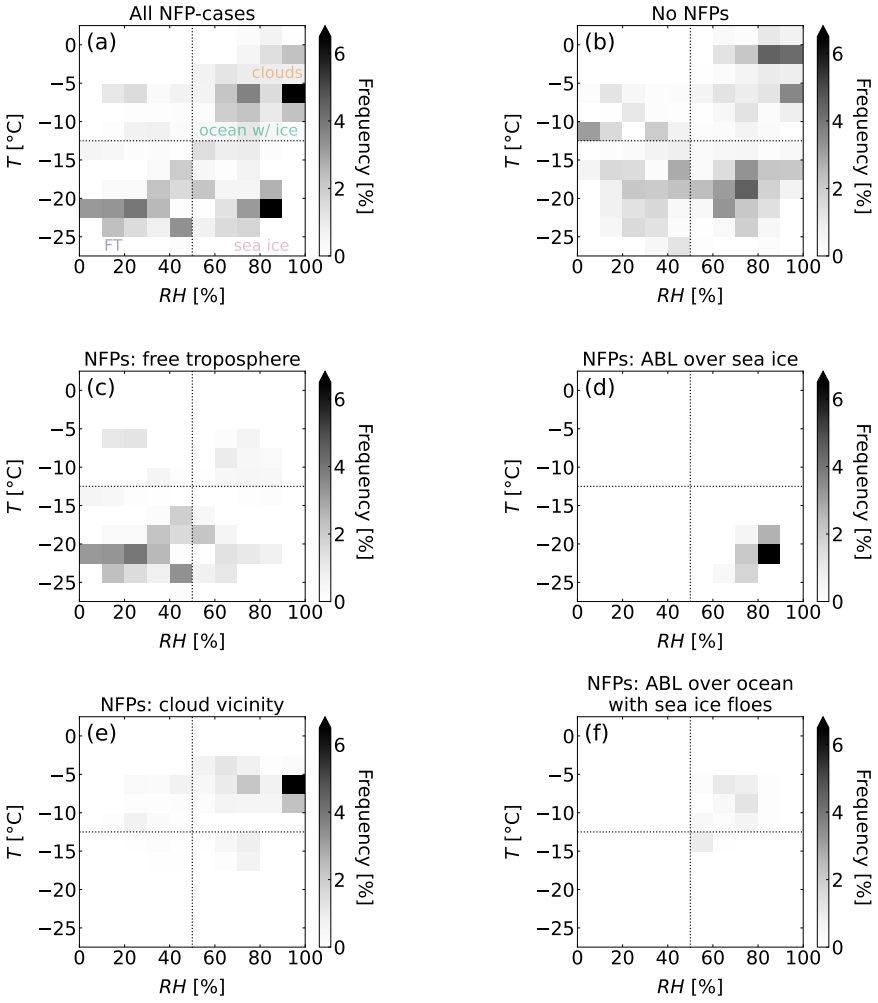


Figure S3. Temperature and relative humidity conditions during **(a)** newly formed particle-cases (NFP-cases) and **(b)** non-NFP-cases. The labels "FT", "sea ice", "clouds", and "ocean w/ ice" in panel (a) denote that within the corresponding quadrant, the measured temperature and relative humidity values are predominantly associated with newly formed particles observed in the free troposphere, the ABL over sea ice, cloud vicinity, and the ABL over ocean with sea ice floes, respectively. The second and third row depict temperature and relative humidity during the occurrence of newly formed particles **(c)** in the free troposphere, **(d)** the ABL over sea ice, **(e)**, the vicinity of clouds, **(f)** and the ABL over ocean with sea ice floes.

during relatively warm, but less humid conditions compared to the observations in cloud vicinity (upper right quadrant in Fig. S3a, Fig. S3f). As the latter cases comprise only about 40 minutes of measurements (6 % of all observations of newly formed particles), the corresponding peaks in Fig. S3f are not strongly pronounced.

As mentioned in Sect. 3.1 in the main text and discussed comprehensively in supporting information (SI) Sect. S5, we found no clear indications ~~for~~ of newly formed particles inside the ABL over open, completely ice-free ocean during our campaign. T-

RH data measured during such observations would likely also feature warm and humid conditions, similar to the data recorded during observations of newly formed particles in the vicinity of clouds and in the ABL over ocean with sea ice floes.

Altogether, these results show that newly formed particles observed during BACSAM II are associated with distinct thermodynamic conditions, which correspond to the different atmospheric scenarios for which newly formed particles were encountered. They include free tropospheric newly formed particles, newly formed particles inside the ABL over sea ice and over ocean with sea ice floes, as well as newly formed particles in the vicinity of clouds. These data provide important information on boundary conditions for laboratory experiments and modeling studies, both of which could facilitate the identification of nucleation mechanisms that might have lead to the presence of newly formed particles, and, furthermore, to assess the broader atmospheric (climate) impact of newly formed particles occurring throughout the lower Arctic troposphere.

S5 Newly formed particles inside the ABL over ocean with sea ice floes

S5.1 Meteorological conditions

During the BACSAM II campaign, we conducted two research flights which included legs inside the ABL over ocean (on 11 and 25 April, Fig. S1). On all other days, the flight sections over open ocean visible in Fig. S1 were carried out above the ABL. On 11 April, we measured PNSDs in a target region in the lee west of Spitsbergen over ocean, with the ocean surface featuring both open water areas and patches of sea ice floes, as well as closed sea ice in the fjord in the proximity of WP7 (Fig. S4a). The air masses probed during the legs inside the ABL originated in sea ice-covered regions north and east of Svalbard (Fig. S4b, c). In the last 24 hours prior to measurements inside the ABL, easterly winds advected cold air over the snow- and ice-covered Svalbard mountains to the target region over ocean (Fig. S4b, c). While mostly clear-sky conditions prevailed, a few scattered clouds were present in the eastern parts of the target region as well (Fig. S4a).

On 25 April, measurements were carried out in a target region southwest of Spitsbergen over open, completely ice-free ocean (Fig. S4d). On this day, air masses approached from southern latitudes (Fig. S4e, f). For the air masses probed inside the ABL (Fig. S4f), an anti-cyclonic flow around Svalbard resulted in north-easterly winds and advection over the sea ice and subsequently over open ocean prior to measurements inside the ABL (Fig. S4f). Air masses probed inside the ABL in the northern section of the target region additionally flowed over the Spitsbergen mountains before approaching the area over open water. In this northern section, sparse scattered cumuli clouds were present, while overcast conditions prevailed in the southern part (Fig. S4d).

S5.2 Particle number size distribution measurements

On 11 April, we carried out flight legs inside the ABL at altitudes of approximately 75 m (from about 9:10 to 9:20 UTC) and 240 m (9:25 to 9:45 UTC) in the northern section of the target region between waypoint 2 (WP2) and WP3 (left y-axis in Fig. S5a, see Fig. S4a for the location of the WPs). One leg was conducted at $\approx$1300 m (9:50 to 10:05 UTC) outside the ABL in the free troposphere. A similar pattern was flown in the southern section between WP4, WP5, WP6 and WP7 (left y-axis in

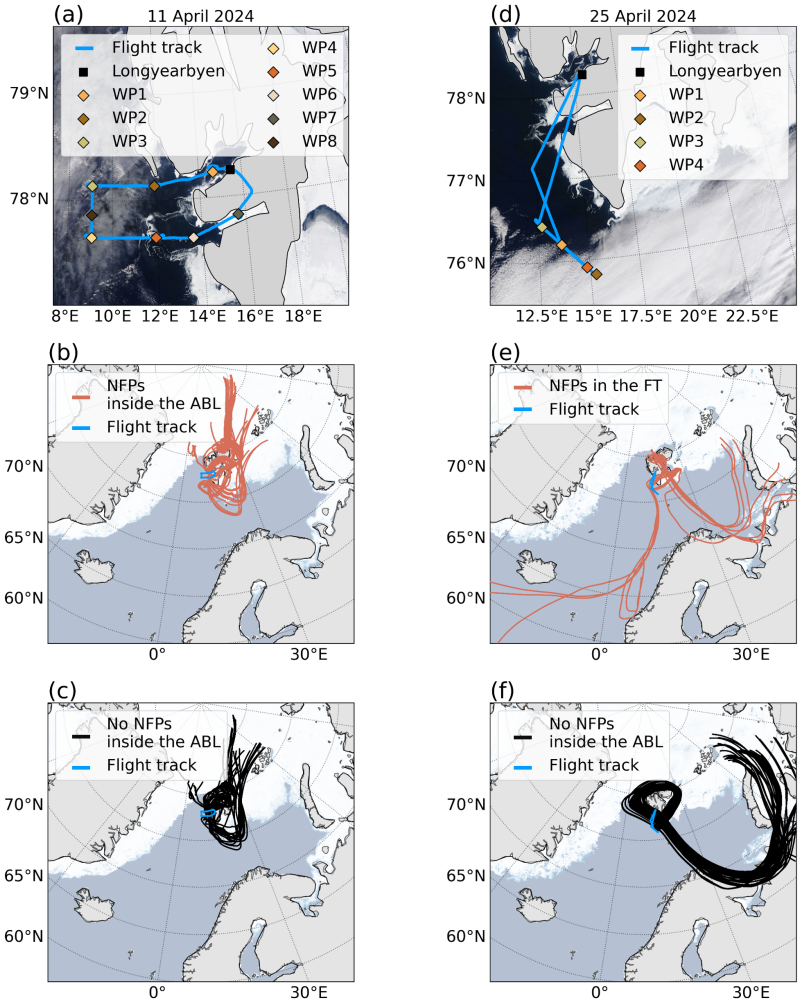


Figure S4. **(a)** Flight track of RF03 on 11 April 2024. **(b)** Five-day backward trajectories associated with newly formed particles (NFPs) inside the ABL on 11 April. **(c)** Five-day backward trajectories connected to PNSD measurements featuring no newly formed particles inside the ABL on 11 April. **(d)** Flight track of RF09 on 25 April 2024. **(e)** Five-day backward trajectories associated with newly formed particles in the free troposphere (FT) on 25 April. **(f)** Five-day backward trajectories connected to PNSD measurements featuring no newly formed particles inside the ABL on 25 April. The MODIS-TERRA satellite images shown in the panels (a) and (d) were retrieved from https://wvs.earthdata.nasa.gov. The sea ice concentration data shown in the subplots (b), (c), (e) and (f) were retrieved from www.seaice.uni-bremen.de (Spreen et al., 2008).

Fig. S5a, see Fig. S4a for the location of the WPs) with legs at ≈1300 m in the free troposphere (10:25 to 10:40 UTC) and inside the ABL at ≈240 m (10:50 to 11:05 UTC), ≈75 m (11:10 to 11:40 UTC), and again at ≈240 m (11:45 to 12:00 UTC). No sea ice was present in the northern section between WP2 and WP3 (Fig. S5a, right y-axis) as shown by ~~a surface temperature~~ surface temperatures below the aircraft of about 3°C. In the southern section between WP4, WP5, WP6, and WP7, the surface contained both open water, scattered sea ice floes, and closed sea ice. This is demonstrated by surface temperatures ranging from about 3°C over open water close to WP4, over −1.8°C close to WP5 and WP6, to −15°C in the fjord close to WP7 (Fig. S5a, right y-axis). As mentioned above, easterly winds prevailed, resulting in off-ice flow, i.e., the areas probed inside the ABL over open water between WP4 and WP5 were located downwind of the sea ice (see Fig. S4b, Fig. S5a).

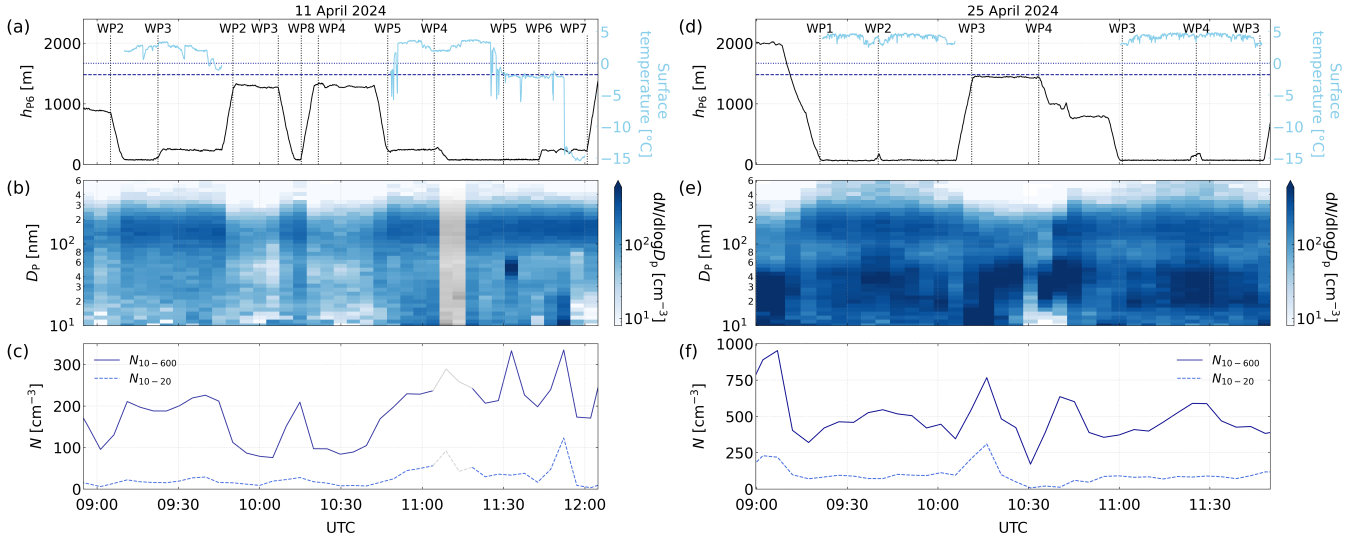


Figure S5. **(a)** P6 altitude during RF03 on 11 April 2024 (black line, left y-axis) as well as surface temperature (blue line, right y-axis). The dashed/dotted blue horizontal lines illustrate a surface temperature of 0°C and the freezing temperature of (salty) Arctic ocean water of −1.8°C. **(b)** MPSS-measured PNSD. The peak in the number concentrations N_{10-600} around 11:32 UTC results from a pollution plume (likely ship exhaust) generating particles with a mode around 60 nm. The measurements from 11:05 to 11:15 UTC are grayed out because the exhaust of the Polar 6 research aircraft was sampled during the turn at WP4. **(c)** Integral particle number concentrations in the total measured size range ($10\ \mathrm{nm} \leq D_\mathrm{p} \leq 600\ \mathrm{nm}$, solid line) and in the nucleation mode size range ($10\ \mathrm{nm} \leq D_\mathrm{p} \leq 20\ \mathrm{nm}$, dashed line), respectively. **(d)** P6 altitude during RF09 on 25 April 2024 (black line, left y-axis) as well as surface temperature (blue line, right y-axis). The dashed/dotted blue horizontal lines illustrate a surface temperature of 0°C and the freezing temperature of Arctic ocean water of −1.8°C. **(e)** MPSS-measured PNSD. **(f)** Integral particle number concentrations in the total measured size range ($10\ \mathrm{nm} \leq D_\mathrm{p} \leq 600\ \mathrm{nm}$, solid line) and in the nucleation mode size range ($10\ \mathrm{nm} \leq D_\mathrm{p} \leq 20\ \mathrm{nm}$, dashed line), respectively. Note the different y-axis between the subplots (c) and (f).

In both the northern and the southern section, particle number concentrations in the size range from 10 nm to 600 nm were increased inside the ABL compared to the free troposphere (Fig. S5b, c). In the northern section, no newly formed particles during the legs inside the ABL over completely ice-free ocean were present (Fig. S5b, c), as indicated by the absence of a

prevailing distinct nucleation mode and rather low number concentrations in the size range from 10 nm to 20 nm ($N_{10-20} \approx 25\,\mathrm{cm}^{-3}$, $\approx 10\,\%$ of the total particle number concentrations measured in the range from 10 nm to 600 nm). One single PNSD measured at 9:30 UTC suggested the presence of a small nucleation mode with a maximum below 10 nm (Fig. S5b). However, because during this measurement a few scattered low-level clouds next to the aircraft were visible in the video data, but their distance to the aircraft could not be quantified and the leg was not carried out directly above/below the cloud top/base, this measurement is assigned to the unclassified category (see Fig. 2 and Fig. 3 in the main text and Sect. S3).

The number concentrations of particles in the nucleation mode size range from 10 nm to 20 nm increased by a factor of roughly two in the southern section inside the ABL over ocean with sea ice floes compared to the northern section (Fig. S5c). Here, $N_{10-20} \approx 50\,\mathrm{cm}^{-3}$, accounting for $\approx 20\,\%$ of the total particle number concentrations measured in the range from 10 nm to 600 nm. Several PNSDs showed a small but clear mode with a maximum below 10 nm (Fig. S5b, around 11:00, 11:15, 11:35, 11:45 UTC), indicative of the presence of newly formed particles. Interestingly, the largest nucleation mode (the highest peak in N_{10-20}) was observed directly at the transition between water with ice floes and closed sea ice in the fjord between WP6 and WP7 around 11:50 UTC (Fig. S5b). The median PNSDs for the legs inside the ABL are shown in Fig. S6 and will be discussed below.

On 25 April, four legs at altitudes of ≈67 m were carried out inside the ABL over open ocean (9:20 to 10:05 UTC and 11:00 to 11:45 UTC, Fig. S5d, left y-axis), i.e., with no sea ice present at all, as shown by ~~a sea surface temperature~~ sea surface temperatures of about 4°C (Fig. S5d, right y-axis). Additionally, one leg was flown at ≈1400 m in the free troposphere between WP3 and WP4 (10:10 to 10:35 UTC). Furthermore, one leg was carried out directly above the decreasing cloud top between WP3 and WP4 at altitudes between about ≈1000 m to ≈750 m (10:35 to 10:55 UTC). During the legs inside the ABL over open water, PNSDs showed no indications regarding the presence of a nucleation mode with a maximum below 10 nm, i.e., no indications ~~for~~ of newly formed particles (Fig. S5e, f). In the free troposphere, around 9:00 UTC and 10:15 UTC, increased numbers of particles in the size range from 10 nm to 20 nm were present, and measured PNSDs indicated the presence of a pronounced nucleation mode. These newly formed particles in the free troposphere were associated with air masses from lower latitudes (Fig. S4e). However, we here focus on the measurements inside the ABL. The occurrence of newly formed particles in the free troposphere is discussed in detail in Sect. 3.2 in the main text.

A more detailed comparison of PNSDs measured during the legs inside the ABL over the Arctic ocean on 11 and 25 April is presented in Fig. S6. The accumulation mode concentrations are similar for all six median distributions depicted therein. Additionally, a sea salt mode was observed during the legs inside the ABL on 25 April (blue distribution in Fig. S6) due to sea spray aerosol (SSA) generation caused by strong winds (horizontal wind speeds of about $15\,\mathrm{m\,s}^{-1}$, strong fluctuations in vertical wind speeds; for a detailed case study on SSA fluxes on 25 April see Simon et al., 2025). The median PNSDs measured inside the ABL over completely ice-free ocean on 11 and 25 April featured no nucleation mode, i.e., no indications ~~for~~ of the presence of newly formed particles were observed (blue and black distributions in Fig. S6). In contrast, PNSDs measured inside the ABL over ~~water~~ ocean with sea ice floes indicated the presence of newly formed particles (red distributions in Fig. S6).

In summary, no ~~clear indications~~ evidence for the occurrence of newly formed particles during measurements inside the ABL

over open, completely ice-free ocean ~~were~~ was found. However, a small number of newly formed particles were detected during measurements inside the ABL over ocean with sea ice floes, i.e., in the direct vicinity and downwind of sea ice.

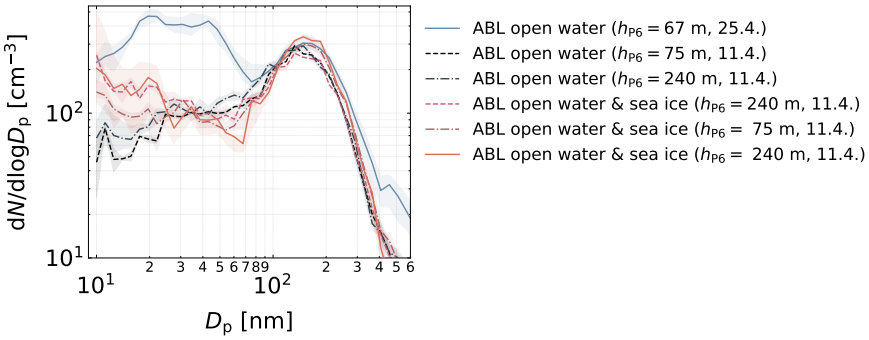


Figure S6. Median particle number size distributions during legs at constant altitude inside the ABL over completely ice-free open water (on 11 and 25 April, black and blue curves) and over ocean with both sea ice floes and open water areas present (on 11 April, red curves). The latter distributions over both open water and sea ice on 11 April are considered as indicative for newly formed particles. The shaded areas represent the interquartile ranges.

S5.3 Chlorophyll-a concentration

We utilized satellite-derived Copernicus Global Ocean Colour data (Gohin et al., 2002; Hu et al., 2012) to carry out an analysis with respect to the chlorophyll-a (chl-a) mass concentration in the sea water during the measurements inside the ABL over ocean on 11 and 25 April. Here, chl-a is treated as a proxy for phytoplankton biomass (Siegel et al., 2013). It is well known that the aerosol precursor dimethylsulfide (DMS) results from the breakdown of dimethylsulfoniopropionate (DMSP), which is produced by phytoplankton (e.g., Simó, 2001; Willis et al., 2017). Thus, we assume that the chl-a concentrations are suited to investigate the potential for the release of DMS from the ocean surface to the atmosphere. In the Arctic at Ny-Ålesund, for example, Beck et al. (2021) showed a good agreement between measured chl-a and DMSP concentrations in seawater, which coincided with a rise in sulfuric acid (SA) and methane sulfonic acid (MSA), both of which are oxidation products of DMS, and the occurrence of new particle formation (NPF) and growth events.

Compared to the background values close to zero, elevated chl-a concentrations are visible in the southern section of the target region on 11 April (Fig. S7a) where both open water and sea ice were present (Fig. S4a, S5a), suggesting that in the sea water in the area probed a phytoplankton bloom occurred. Furthermore, the data show no or only slightly increased chl-a concentrations in the northern section (Fig. S7a).

Fig. S7b depicts the backward trajectories inside the ABL on 11 April. We restrict the following discussion to air masses which resided inside the ABL since we expect that only those air masses could have picked up precursor gases from the ocean surface, whereas an influence of emissions from the surface on free tropospheric air masses is unlikely. Consequently, only the parts of the trajectories inside the ABL are shown in Fig. S7b-d, f-h. As mentioned above, easterly winds prevailed in both the northern and the southern section (Fig. S7b). The air masses sampled in the northern section, for which no newly formed particles were

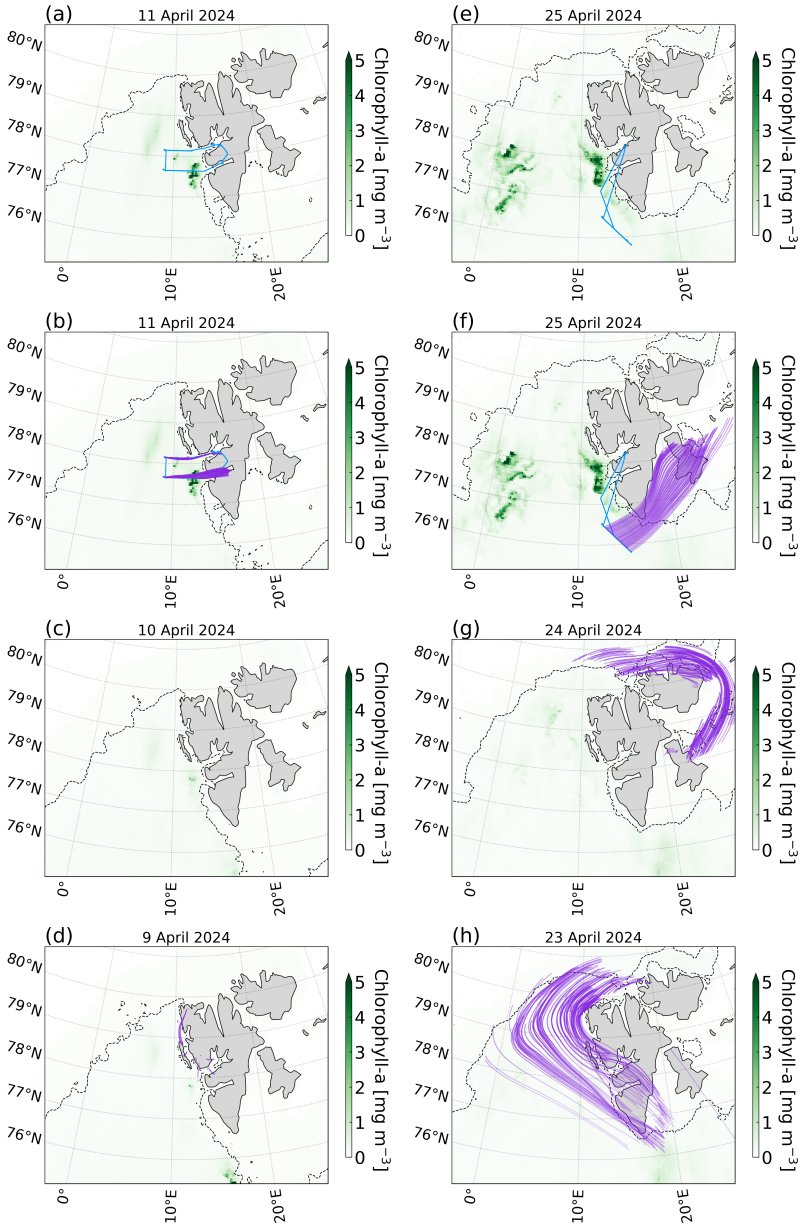


Figure S7. Flight track (blue), backward trajectories inside the ABL (violet), and chlorophyll-a mass concentrations (green) based on Copernicus-GlobColour data (Gohin et al., 2002; Hu et al., 2012) for the research flights featuring measurements inside the ABL over ocean on 11 and 25 April. The left column depicts the chlorophyll-a concentrations for 11 April 2024 and the two preceding days. Similarly, the right column depicts the chlorophyll-a concentrations for 25 April 2024 and the two preceding days. For convenience, only the respective flight tracks and chlorophyll-a concentrations for the days of the research flights are shown in the first row in panels (a) and (e). In the panels (b), (d), (d), (f), (g), and (h), the backward trajectories during the corresponding days are depicted as well. Only trajectories inside the ABL are shown, i.e., if no trajectory data are shown such as in panel (c) or gaps in the trajectories are visible such as in (d), (g), and (h), the trajectories did not reside inside the ABL at these geographical positions. The dashed black line in all subplots illustrates the sea ice extent based on 15 % sea ice concentration (Spreen et al., 2008).

observed, did not pass over ocean surfaces featuring enhanced chl-a concentrations (Fig. S7b). In contrast, in the southern section, measurements in the direct vicinity of ocean waters with increased chl-a were conducted, as well as measurements downwind of these areas indicative of a phytoplankton bloom. On the two previous days, the air massed resided completely (10 April, Fig. S7c) and overwhelmingly outside of the ABL (9 April, Fig. S7d), limiting the possibility for precursor uptake from the (ocean) surface on those days. This suggests that the presumed emission of precursors, potentially leading to NPF and the occurrence of newly formed particles in the southern section of the target area on 11 April, occurred rather locally.

In the area probed on 25 April, the chl-a data showed no indications ~~for~~ of a phytoplankton bloom (Fig. S7e). Similarly, in the areas where backward trajectories resided inside the ABL during 25 April and the two preceding days, no elevated chl-a concentrations were present in the sea water (Fig. S7f-h).

In summary, no evidence for a phytoplankton bloom in the northern section of the area probed on 11 April and in the area probed on 25 April was found based on the satellite data. However, in the southern section of the target region investigated on 11 April, the chl-a data suggest that a phytoplankton plume occurred. This might explain why newly formed particles were found inside the ABL over ocean with sea ice floes above and downwind of the plume area and the sea ice, but no newly formed particles were detected during the measurements inside the ABL over completely ice-free ocean. However, the occurrence of newly formed particles between WP6 and WP7 (Fig. S5a-c) upwind of the plume area on April 11 was likely not affected by the chl-a plume as the wind direction would prevent the eastward transport of possibly emitted precursors (Fig. S7b). Due to the absence of gas phase measurements, we cannot ultimately resolve if the potential release of precursors such as DMS from the sea surface and its possible participation in NPF might have contributed to the occurrence of newly formed particles on 11 April. Hence, we can only speculate that the presence of newly formed particles over ocean with sea ice floes on this day might be related to emissions of precursors from the open water or the sea ice, or both. Another potential explanation has been initially proposed by Leck and Bigg (1999, 2010) who suggested that the fragmentation of marine organic polymer gels led to the appearance of particles in the nucleation mode size range. Such events often involved the dissipation of cloud or fog droplets, emitting particles with sizes of a few nanometers to the atmosphere (Leck and Bigg, 1999, 2010; Karl et al., 2013; Leck et al., 2025).

S6 New and recently formed particles in the free troposphere

Fig. S8 shows the median PNSD and corresponding interquartile range of all PNSD-measurements indicative of newly formed particles during the transit to Villum research station in the free troposphere (13 April 2024, RF04, Sect. 3.2 in the main text). These data were recorded during the time period 6:23 to 7:07 UTC and 7:17 to 7:40 UTC.

Two PNSDs measured in the time period from 7:07 to 7:17 UTC peaked at about 18 nm and showed no indications concerning a mode featuring a maximum below 10 nm (Fig. S8). According to our criteria defined in Sect. 2.2 in the main text, these PNSDs are not considered as indicative for newly formed particles. We rather interpret them as steming from "recent particle formation" (RPF), since the small particle sizes still suggest that these particles must originate from secondary particle production (e.g.,

Kulmala et al., 2004). Such recently formed particles are excluded from further analysis and we here focus solely on newly formed particles. Investigating recently formed particles in more detail is beyond the scope of this paper.

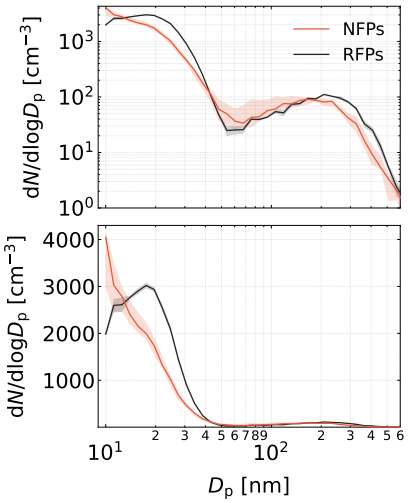


Figure S8. Median PNSD of measurements indicative of newly formed particles (NFPs) and recently formed particles (RFPs, solid lines) observed on 13 April 2024 during the transit from Longyearbyen to Villum Research Station (case study on newly formed particles in the free troposphere). The shaded areas represent the interquartile ranges.

S7 Newly formed particles in the atmospheric boundary layer over sea ice

S7.1 Sea ice conditions

To illustrate the sea ice conditions prevailing in the target region east of Svalbard between WP1 and WP3 on 15 April 2024 (RF05, Sect. 3.3 in the main text), Fig. S9 displays examples of fisheye camera images facing downward from the P6 aircraft during the legs inside the ABL. Leads and cracks in the sea ice are visible.

S7.2 Vertical profile

From the inversion observed in the vertical profiles of potential temperature (Θ) between WP1 and WP3, we determine the ABL height (Fig. S10). The solid line in Fig. S10 shows the mean Θ-profile averaged over the four ascents/descents at WP1, WP2, and WP3 (see Fig. 8a in the main text). The shaded area represents the standard deviation and thus the variability between the individual ascents/descents. The data have been grouped into altitude bins with a width of 20 m before averaging. The markers with errorbars show mean values and standard deviations derived from the measurements during the horizontal legs. The horizontal dashed lines represent the average aircraft altitude during these low-level legs (at $\approx 70\,\mathrm{m}$ and $\approx 155\,\mathrm{m}$) close to the

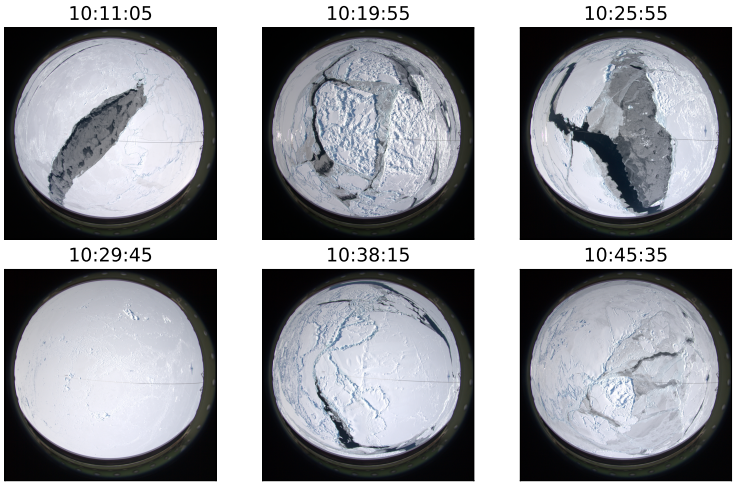


Figure S9. Sea ice conditions during RF05 on 15 April 2024 (case study in the ABL over sea ice). The title denotes the time in UTC.

surface inside the ABL ($h_{\mathrm{P6,\,inside\,BL}}$) and the high-level leg above the ABL in the free troposphere ($h_{\mathrm{P6,\,outside\,BL}} \approx 850\,\mathrm{m}$). In Fig. S10, an inversion at an altitude of about 190 m can be identified for the target region.

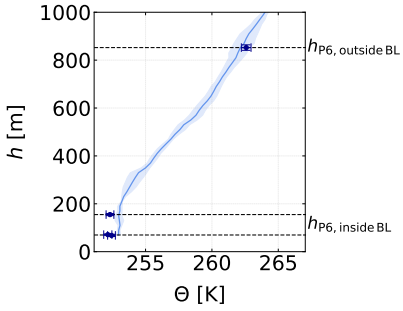


Figure S10. Mean vertical profile of potential temperature for the case study in the ABL over sea ice on 15 April 2024, derived from the ascents/descents (solid line). The shaded area represents the standard deviation. The markers with errorbars show mean values and standard deviations derived from the measurements during the horizontal legs. The horizontal dashed lines illustrate the average aircraft altitude during these legs.

S7.3 Particle number size distributions

245 Fig. S11 shows the median PNSDs measured during the three consecutive legs carried out in the same area and at constant altitude between WP1 and WP3 (see Fig. 8a in the main text) inside the ABL over sea ice. ABL 1 refers to the first leg flown inside the ABL at an altitude of $\approx 70\,\mathrm{m}$ (10:15 to 10:47 UTC), ABL 2 to the second leg at $\approx 155\,\mathrm{m}$ (10:58 to 11:25 UTC), and

ABL 3 to the third leg, again at ≈ 70 m (12:13 to 12:43 UTC). The decrease with time of the number concentration in the size range below 20 nm is clearly visible.

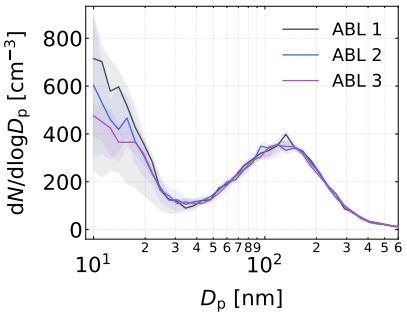


Figure S11. Median PNSDs (solid lines) and corresponding interquartile ranges (shaded areas) for the legs at ≈ 70 m (ABL 1 and ABL 3) and ≈ 155 m (ABL 2) inside the ABL over sea ice on 15 April 2024.

S8 Newly formed particles in the vicinity of clouds

S8.1 Sea ice conditions

To illustrate the sea ice conditions prevailing in the target region north of Svalbard between WP1 and WP2 on 24 April 2024 (RF08, Sect. 3.4 in the main text), Fig. S12 displays examples of fisheye camera images facing downward from the P6 aircraft during the leg at cloud base. Leads and cracks in the sea ice are visible.

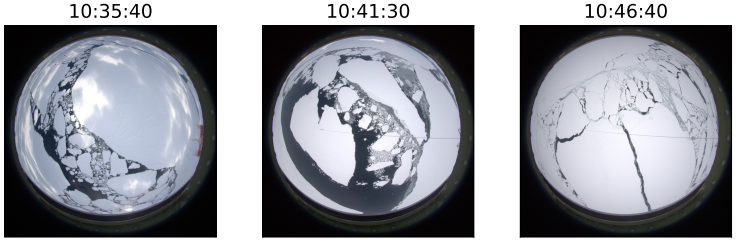


Figure S12. Sea ice conditions during RF08 on 24 April 2024 (case study in the vicinity of clouds). The title denotes the time in UTC.

S8.2 Vertical profiles

For the case study on newly formed particles in the vicinity of clouds, the ascent through cloud (10:52 to 10:58 UTC, see Fig. 11a in the main text) is excluded from analysis with respect to the aerosol particle measurements, because erroneous measurements due to icing of the aerosol inlet and/or droplet shattering cannot be ruled out (Weber et al., 1998). Nevertheless, temperature and pressure data recorded during the ascent can with caution be used to determine vertical profiles of potential

temperature to investigate the stratification in the target region. In Fig. S13, we show the potential temperature derived from these data collected during the ascent through cloud (see Fig. 11a in the main text). Directly in the target region between WP1 and WP2 (see Fig. 10a in the main text), no vertical profiling down to the lowest possible flight altitude was carried out. Therefore, in addition, the potential temperature derived from a vertical profile down to $\approx 80\,\mathrm{m}$, which was conducted after passing WP2 and while returning toward the sea ice edge (see Fig. 10(a) in the main text), is depicted in Fig. S13. Here, the solid line represents the mean, averaged over ascent and descent, and the shaded area the corresponding standard deviation. Additionally, we show the potential temperature profile in the target region between WP1 and WP2 based on Copernicus Arctic Regional Reanalysis (CARRA) data. Cloud top and base, illustrated by the shaded gray area representing the cloud in Fig. S13, were determined from the profile of potential temperature and from in situ video data. Both CARRA and in situ data show an inversion below the cloud, which suggests that in the area probed between WP1 and WP2, the clouds were decoupled from the surface.

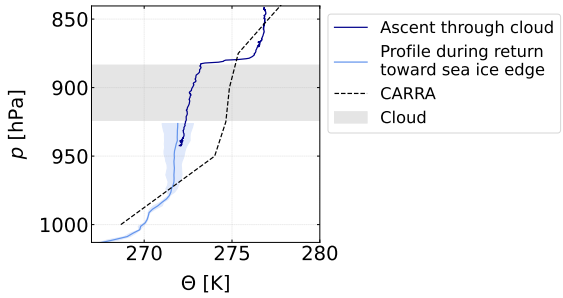


Figure S13. Vertical profile of potential temperature for the case study in the vicinity of clouds on 24 April 2024, derived from in situ data collected during ascents/descents (solid lines) as well as based on CARRA reanalysis data (dashed line).

S8.3 Cloud top radiative cooling

We further utilize the ascent through the cloud to determine the radiative heating/cooling rates in an atmospheric layer between two flight altitudes, with $z_{\mathrm{bottom/top}}$ denoting the altitudes at the bottom/top of this layer (Lonardi et al., 2024). Following Lonardi et al. (2024), we calculate the heating/cooling rates as

$$\zeta = \frac{1}{\rho c_{\mathrm{p}}} \frac{F_{\mathrm{net}}(z_{\mathrm{top}}) - F_{\mathrm{net}}(z_{\mathrm{bottom}})}{z_{\mathrm{top}} - z_{\mathrm{bottom}}}, \tag{1}$$

where ρ and c_{p} are density and specific heat capacity at constant pressure of air, and $F_{\mathrm{net}}(z)$ the net thermal irradiance at flight altitude z. Positive/negative values in ζ indicate radiative heating/cooling (Lonardi et al., 2024). The heating/cooling rates are plotted in Fig. S14, which shows a sharp minium at about 1150 m, i.e., radiative cooling at the cloud top.

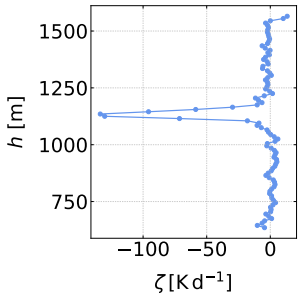


Figure S14. Radiative heating/cooling rates for the case study in the vicinity of clouds on 24 April 2024, determined from the ascent through cloud.

Data availability. Master tracks are available on PANGAEA for all research flights of the BACSAM II campaign (Jurányi et al., 2024). Backward trajectory data are available on PANGAEA for all research flights of the BACSAM II campaign (Kirbus and Wendisch, 2024). PNSD data from all research flights of the BACSAM II campaign are available on PANGAEA (Simon et al., 2026). Sea ice data were retrieved from www.seaice.uni-bremen.de (Spreen et al., 2008). MODIS-TERRA satellite images were retrieved from https://wvs.earthdata.nasa.gov. This study has been conducted using E.U. Copernicus Marine Service Information; https://www.doi.org/10.48670/moi-00281.

Author contributions. DJS participated in the data collection and flight planning during the BACSAM II campaign, analyzed and interpreted the data, and wrote the manuscript. JS participated in the data collection and flight planning, discussed the data, and contributed to the writing. JH participated in the data collection and flight planning, and processed the position, nose boom, and humidity data. BK performed the trajectory calculations and supported their analysis. JM participated in the data collection, flight planning, and calculated the radiative heating/cooling rates. ZJ, MH, BW, LK,AMJ, and MW participated in the flight planning, and the data collection and related discussions. KW was responsible for the development of the MPSS system. AH and ZJ functioned as PIs during the campaign. AH, ZJ, SH, GCR, MW, and MLP contributed to the discussion of the results. FS conceived the study, functioned as PI during the campaign, and contributed to data interpretation and writing. All authors read and edited the manuscript.

Competing interests. The authors declare no competing interests.

Acknowledgements. We gratefully acknowledge the funding by the Deutsche Forschungsgemeinschaft (DFG, German Research Foundation) – Project Number 268020496 – TRR 172, within the framework of the Transregional Collaborative Research Center "ArctiC Amplification: Climate Relevant Atmospheric and SurfaCe Processes, and Feedback Mechanisms (AC)^3", as well as the support of the Alfred-Wegener-Institute, Helmholtz Centre for Polar and Marine Research through grant number AWI_PA_02172. The authors used ~~a large language model~~ large language models (ChatGPT by OpenAI, Claude by Anthropic) solely to support coding tasks; all scientific reasoning, methodological decisions, analyses, and conclusions were developed independently by the authors.

References

Baron, P. A. and Willeke, K.: Aerosol Measurement: Principles, Techniques, and Applications: [2001], John Wiley and Sons, 2001.

Beck, L. J., Sarnela, N., Junninen, H., Hoppe, C. J., Garmash, O., Bianchi, F., Riva, M., Rose, C., Peräkylä, O., Wimmer, D., et al.: Differing mechanisms of new particle formation at two Arctic sites, Geophysical Research Letters, 48, e2020GL091 334, https://doi.org/10.1029/2020GL091334, 2021.

Gohin, F., Druon, J. N., and Lampert, L.: A five channel chlorophyll concentration algorithm applied to SeaWiFS data processed by SeaDAS in coastal waters, International Journal of Remote Sensing, 23, 1639–1661, https://doi.org/10.1080/01431160110071879, 2002.

Hu, C., Lee, Z., and Franz, B.: Chlorophyll aalgorithms for oligotrophic oceans: A novel approach based on three-band reflectance difference, Journal of Geophysical Research: Oceans, 117, https://doi.org/https://doi.org/10.1029/2011JC007395, 2012.

Jurányi, Z., Stratmann, F., Herber, A., Wendisch, M., and Borrmann, S.: Master tracks in different resolutions during POLAR 6 campaign P6-247_BACSAM2_2024, https://doi.org/10.1594/PANGAEA.971763, 2024.

Jurányi, Z., Lüpkes, C., Stratmann, F., Hartmann, J., Schaefer, J., Jörss, A.-M., Schulz, A., Wetzel, B., Simon, D., Gebhard, E., Stöhr, M., Hofmann, P., Kalmbach, D., Grawe, S., Wendisch, M., and Herber, A.: The T-Bird – a new aircraft-towed instrument platform to measure aerosol properties and turbulence close to the surface: introduction to the aerosol measurement system, Atmospheric Measurement Techniques, 18, 3477–3494, https://doi.org/10.5194/amt-18-3477-2025, 2025.

Karl, M., Leck, C., Coz, E., and Heintzenberg, J.: Marine nanogels as a source of atmospheric nanoparticles in the high Arctic, Geophysical Research Letters, 40, 3738–3743, https://doi.org/https://doi.org/10.1002/grl.50661, 2013.

Kirbus, B. and Wendisch, M.: Five-day backwards trajectories at one minute resolution along the flight tracks of the Polar 6 research aircraft during BACSAM II, https://doi.org/10.1594/PANGAEA.971694, 2024.

Kulmala, M., Vehkamäki, H., Petäjä, T., Dal Maso, M., Lauri, A., Kerminen, V.-M., Birmili, W., and McMurry, P.: Formation and growth rates of ultrafine atmospheric particles: a review of observations, Journal of Aerosol Science, 35, 143–176, https://doi.org/10.1016/j.jaerosci.2003.10.003, 2004.

Leck, C. and Bigg, E. K.: Aerosol production over remote marine areas-A new route, Geophysical Research Letters, 26, 3577–3580, https://doi.org/https://doi.org/10.1029/1999GL010807, 1999.

Leck, C. and Bigg, E. K.: New Particle Formation of Marine Biological Origin, Aerosol Science and Technology, 44, 570–577, https://doi.org/10.1080/02786826.2010.481222, 2010.

Leck, C., Heintzenberg, J., Nygård, T., and Naakka, T.: Is the summer aerosol over the Arctic controlled by regional atmospheric circulation or ice conditions? Trends and future implications, Atmospheric Chemistry and Physics, 25, 16 775–16 795, https://doi.org/10.5194/acp-25-16775-2025, 2025.

Lonardi, M., Akansu, E. F., Ehrlich, A., Mazzola, M., Pilz, C., Shupe, M. D., Siebert, H., and Wendisch, M.: Tethered balloon-borne observations of thermal-infrared irradiance and cooling rate profiles in the Arctic atmospheric boundary layer, Atmospheric Chemistry and Physics, 24, 1961–1978, https://doi.org/10.5194/acp-24-1961-2024, 2024.

McFarquhar, G. M. and Cober, S. G.: Single-scattering properties of mixed-phase Arctic clouds at solar wavelengths: Impacts on radiative transfer, Journal of Climate, 17, 3799–3813, https://doi.org/10.1175/1520-0442(2004)017<3799:SPOMAC>2.0.CO;2, 2004.

Moser, M., Voigt, C., Jurkat-Witschas, T., Hahn, V., Mioche, G., Jourdan, O., Dupuy, R., Gourbeyre, C., Schwarzenboeck, A., Lucke, J., Boose, Y., Mech, M., Borrmann, S., Ehrlich, A., Herber, A., Lüpkes, C., and Wendisch, M.: Microphysical and thermodynamic phase

analyses of Arctic low-level clouds measured above the sea ice and the open ocean in spring and summer, Atmospheric Chemistry and Physics, 23, 7257–7280, https://doi.org/10.5194/acp-23-7257-2023, 2023.

Seinfeld, J. H. and Pandis, S. N.: Atmospheric chemistry and physics: from air pollution to climate change, John Wiley & Sons, 2006.

Siegel, D. A., Behrenfeld, M. J., Maritorena, S., McClain, C. R., Antoine, D., Bailey, S. W., Bontempi, P. S., Boss, E. S., Dierssen, H. M., Doney, S. C., et al.: Regional to global assessments of phytoplankton dynamics from the SeaWiFS mission, Remote Sensing of Environment, 135, 77–91, 2013.

Simó, R.: Production of atmospheric sulfur by oceanic plankton: biogeochemical, ecological and evolutionary links, Trends in Ecology & Evolution, 16, 287–294, 2001.

Simon, D. J., Hartmann, J., Schaefer, J., Zeppenfeld, S., Lüpkes, C., Hartmann, M., Wetzel, B., Heinold, B., Jurányi, Z., Schulz, A., et al.: Turbulent Aerosol fluxes from airborne measurements over the Arctic Ocean, Geophysical Research Letters, 52, e2025GL117 094, https://doi.org/10.1029/2025GL117094, 2025.

Simon, D. J., Schaefer, J., Hartmann, M., Weinhold, K., and Stratmann, F.: Airborne in-situ measurements of aerosol particle number size distributions during the BACSAM II campaign in April 2024, https://doi.org/10.1594/PANGAEA.993546, 2026.

Spreen, G., Kaleschke, L., and Heygster, G.: Sea ice remote sensing using AMSR-E 89-GHz channels, Journal of Geophysical Research: Oceans, 113, https://doi.org/10.1029/2005JC003384, 2008.

Von der Weiden, S.-L., Drewnick, F., and Borrmann, S.: Particle Loss Calculator–a new software tool for the assessment of the performance of aerosol inlet systems, Atmospheric Measurement Techniques, 2, 479–494, https://doi.org/10.5194/amt-2-479-2009, 2009.

Weber, R., Clarke, A., Litchy, M., Li, J., Kok, G., Schillawski, R., and McMurry, P.: Spurious aerosol measurements when sampling from aircraft in the vicinity of clouds, Journal of Geophysical Research: Atmospheres, 103, 28 337–28 346, https://doi.org/10.1029/98JD02086, 1998.

Willis, M. D., Köllner, F., Burkart, J., Bozem, H., Thomas, J. L., Schneider, J., Aliabadi, A. A., Hoor, P. M., Schulz, H., Herber, A. B., et al.: Evidence for marine biogenic influence on summertime Arctic aerosol, Geophysical Research Letters, 44, 6460–6470, https://doi.org/10.1002/2017GL073359, 2017.